UNIVERSITÉ DU QUÉBEC À MONTRÉAL

# OPTIMISER LES PERFORMANCES DU CAPTEUR DE MASSE ACOUSTIQUE À ONDE DE LAMB EN AJUSTANT LE RAPPORT DE MÉTALLISATION DE L'ÉLECTRODE DE TRANSDUCTION

MÉMOIRE

PRÉSENTÉ

COMME EXIGENCE PARTIELLE

DE LA MAÎTRISE EN GÉNIE ÉLECTRIQUE

PAR

FATEMEH GHOLAMI

JANVIER 2023

# ACKNOWLEDGMENTS

This project would not have been possible without the support of many people. I would like to express my sincere gratitude to my supervisor Prof. Paul-Vahé Cicek. I am very grateful for the confidence he gave me during this project, his scientific advice, technical assistance, insightful suggestions, and financial support throughout my research. I also wish to thank my co-advisor Prof. Alexandre Robichaud for his assistance, comments, methodological guidance, and his brilliant ideas. Thank you both for these years of master which have been excellent for me. I appreciate UQAM and its employees for providing the facilities required for this project.

These years would not have been so enjoyable without my dear husband Milad. Thank you for all your kindness and support throughout this adventure and for accompanying me during all these years' successes and challenges.

I want to thank my mother for her strong support during my childhood and especially my father who was miles away from me but was always there whenever I needed academic or emotional support.

I am also grateful to my dear friend Maryam for her constant presence, which made me feel less away from my family. It was my pleasure to working with and learning from my colleague Simon Dallaire, I appreciate his useful discussions and suggestions.

TABLE OF CONTENTS

# LIST OF TABLES

LIST OF FIGURES

# ABSTRACT

In this thesis, theory and application of numerous acoustic biosensors with different types of wave propagation properties is reviewed. Specifically, we investigated the resonator design and the impact of interdigital transducer (IDT) structure and piezoelectric thickness on a Lamb wave biosensor properties. In order to achieve reliable results, multiple time-domain and frequency-domain simulations have been performed. The CMOS-based technology provided by SilTerra, served as the basis for the parameters and topological choices used for this lamb wave biosensor, and yielded a mass sensitivity of roughly 114 [$cm^2/gr$]. According to the design requirements, we observed that the metallization ratio can be successfully tuned in order to provide the best possible tradeoff between transmission gain and sensitivity. Furthermore, we found that applying a differential input configuration to the IDT electrodes can provide a 20% transmission gain improvement in comparison to the single-ended configuration. We also demonstrated that the $Si_3N_4$ layer present in the SilTerra technology can be effectively harnessed as a guiding layer to boost transmission gain by a factor of five. After investigating the THD level at various IDT metallization ratios, we observed that THD is extremely low at all ratios, and is not a worthy source of concern in the selection of an optimal metallization ratio.

# RÉSUMÉ

Dans ce projet de recherche, la théorie et l'application de nombreux biocapteurs acoustiques avec différents types de propagation des ondes sont passées en revue. Plus précisément, nous avons étudié la conception du résonateur et l'impact de la structure des IDTs et de l'épaisseur du piézoélectrique sur les propriétés d'un biocapteur à onde de Lamb. Afin d'obtenir des résultats fiables, plusieurs simulations dans le domaine temporel et fréquentiel ont été réalisées. La technologie basée sur CMOS fournie par SilTerra, a servi de base aux paramètres et aux choix de designes utilisés pour ce biocapteur à ondes de Lamb, et a donné une sensibilité de masse d'environ 114 [$cm^2$/gr]. Selon les exigences de conception, nous avons observé que le rapport de métallisation peut être mis au point avec succès afin de fournir le meilleur compromis possible entre le gain de transmission et la sensibilité. De plus, nous avons constaté que l'application d'une configuration d'entrée différentielle aux électrodes peut fournir une amélioration du gain de transmission de 20% par rapport à la configuration single ended. Nous avons également démontré que la couche $Si_3N_4$ présente dans la technologie SilTerra peut être efficacement exploitée en tant que couche guidante pour multiplier par cinq le gain de transmission. Après avoir étudié le niveau de THD à divers rapports de métallisation IDT, nous avons observé que le THD est extrêmement faible à tous les rapports et n'est pas une source digne de préoccupation dans la sélection d'un rapport de métallisation optimal.

# CHAPTER I

# INTRODUCTION

Whether in a research environment or a medical laboratory testing, we need accurate devices to detect and quantify the amount of certain particles. The presence of biological particles can be determined or measured using biosensors that make quick experiments possible. Micro biosensors are interesting because of their ability to be used in lab on chips (LOC). To monitor a drug's efficacy, a LOC might be placed on the patient to provide the right dosage considering their condition, providing customized medication. Highly accurate and sensitive biosensors are needed to ensure reliability in real-world applications, especially when diagnosing diseases. One of the most precise biosensors is the acoustic type based on mechanical vibrations. Different acoustic biosensors are characterized according to their propagating wave. The two most frequently employed waves for sensing applications are the shear horizontal (SH-H) acoustic wave (Martin et al., 1989) and the Lamb wave that can either operate at antisymmetric (A0) (Yantchev et al., 2011) or symmetric (S0) (Yantchev et al., 2012) modes. To stimulate a wave propagating with Lamb or SH-H wave characteristics, the right material type, crystal cut, and wave propagation direction should be chosen, as shown theoretically and empirically by Moriizumi et al. (1987). In recent years, Lamb wave resonators based on sputtered aluminum nitride (AlN) thin films have shown promising results for high-frequency applications up to several gigahertz (GHz), various resonance

frequencies on a single chip, and fabrication compatibility with CMOS circuits. Among different sensor properties, the interdigital transducer (IDT) geometry is a determinant factor in mass-sensitive acoustic devices. The number, width, length, and form of IDTs impact device behavior, wave propagation, and mass sensitivity (Wohltjen, 1984; Skinner et al., 2006). The effects of IDT finger length on synthesizing acoustic plate waves were assessed by Wohltjen (1984). In a lamb wave resonator made of aluminum nitride (AlN), Lin et al. (2014) used the symmetric mode to examine the effects of various electrode materials, transducer configurations, and electrode thicknesses on the coupling factor.

## 1.1 Applications

As mentioned above, biosensors are instruments used to measure the concentration or presence of a biological analyte, such as microorganisms, biological structures, or biomolecules. Environment and Health are the main industries that can benefit from the advent of biosensors. As an example of environmental use, a surface acoustic wave microfluidic chip created by Tamarin et al. enables the evaluation of water quality outside a laboratory environment (Tamarin et al., 2020). A reliable biosensor that could identify the mycobacterial antigen in biological fluids would be very helpful. An example of a noninvasive screening procedure for high-risk people is antigen detection in saliva (Kumar et al., 2000). Gray et al. provided a biosensor for the quick detection of HIV in biological fluids, which is an important step (Gray et al., 2018). Numerous studies have demonstrated that employing acoustic biosensors speeds up diagnosis and improves accuracy. For the purpose of detecting the hepatitis B virus, a Quartz crystal microbalance (QCM) based biosensor with gold electrodes was built on the foundation of an AT cut with a fundamental frequency of 9 MHz (Pohanka, 2017).

## 1.2 Contributions

Lamb wave biosensors present several advantages, including higher resonance frequency leading to higher sensitivity, the possibility of multiple mode propagation with various characteristics that can be used for different sensor applications, simplicity of CMOS technology integration, and their suitability in being utilized in liquid environments. As previously stated, a mass sensor integrated with CMOS technology has several advantages, including ease of use in liquid areas, this fact led us to use SilTerra's CMOS technology to design and simulate a mass-sensitive Lamb wave microsensor. The effects of changing the metallization ratio on the transmission gain, total harmonic distortion (THD), and two distinct resonant modes are demonstrated. Depending on the design criteria, it has been discovered that the metallization ratio can be designed to achieve an optimal tradeoff between transmission gain and sensitivity. Improving sensitivity and minimizing insertion loss are two important goals for a mass sensor, which led us to investigate the effects of various IDT metallization ratios and signal application techniques on these characteristics. The mass sensitivity of the lamb wave designed with Silterra's dimensions is around 114 $cm^2/gr$. The device's transmission gain is increased five times by adding a $Si_3N_4$ layer on top. The transmission gain of the differential IDT configuration was also investigated to be 20% more efficient than a single terminal.

## 1.3 Organisation

There are four chapters in this thesis. The project's motivations, applications, and contributions are introduced in the present chapter.

Chapter 2 reviews the concepts of several acoustic biosensors with various waves, describes the configurations of resonators and illustrates the effect of thickness on

the sensitivity of the biosensor.

Chapter 3 is an article published in the journal MDPI SENSORS, which presents simulations to improve lamb wave acoustic mass sensor performance by adjusting the transduction electrode metallization ratio.

The thesis conclusions and recommended future research are presented in Chapter 4.

## 1.4 Publications

Gholami, F., Shih, A., Robichaud, A. et Cicek, P.-V. (2022). A study of optimizing lamb wave acoustic mass sensorsrsquo ; performance through adjustment of the transduction electrode metallization ratio. Sensors, 22(17)

# CHAPTER II

# LITERATURE REVIEW

## 2.1 Introduction

There exist various acoustic microsensors with multiple applications and fabrication techniques ; their main point in common is that they use piezoelectric materials to generate acoustic waves in the sensor's substrate. Piezo-electric crystals experience a mechanical deformation under the influence of an electric field and vice versa. Acoustic biosensors are created and named depending on the kind of acoustic wave which is propagating such as Bulk Acoustic Wave (BAW), Film Bulk Acoustic Resonator (FBAR), and Surface Acoustic Wave (SAW) biosensors. Bulk micromachining and surface micromachining are the two micromachining techniques used to create these devices in order to give the materials a certain shape (Adams and Layton, 2009). In a nutshell, surface micromachining does not alter the substrate : it refers to adding a stack of material layers on top of the substrate. Alternatively, bulk micromachining involves shaping the substrate by removing materials by etching from the substrate to build the structure. The Film Bulk Acoustic Resonator (FBAR) is an example of a resonator made by the bulk micromachining methods.

Beginning with the basic ideas behind acoustic biosensors, this chapter goes on to discuss most types of acoustic biosensors. The methods of immobilization and mass

sensing are covered in the following subchapter. It is also discussed how interdigital transducers (IDTs) are utilized to electrically excite elastic wave propagation in piezoelectric substrates. Finally, the effect of layer thickness on the biosensor is discussed in the last subchapter.

## 2.2 Acoustic resonators

An acoustic biosensor is a device with a transducer built on a solid piezoelectric slab that produces a standing wave in the substrate of the sensor by combining a traveling wave with confinement ; the frequency of the standing wave is determined by the velocity of the progressive wave (Lucklum et al., 2004). Two main waveforms are recognized in a medium, transversal (shear), and longitudinal (compressional/extensional) wave. A longitudinal (compressional/extensional) wave is one in which a particle's motion is parallel to the wave propagation, whereas a transversal (shear) wave is one in which a particle's motion is perpendicular to the wave propagation. There are two wave propagation models in a piezoelectric crystal resonator ; Bulk acoustic wave (BAW) propagation, in which the wave is traveling in the entire substrate, and Surface acoustic wave (SAW), in which the wave is traveling on the surface of the substrate. Due to their lower viscous loss, BAW resonators are appropriate for liquid-based detection. These devices demonstrate good performance by their high quality factors compared to their flexural counterparts (Prasad et al., 2015). In the following, seven different types of biosensors are explored.

### 2.2.1 Quartz crystal microbalance Sensors (QCM)

QCM sensors have two cylindrical electrodes positioned on both ends of the crystal with a special piezoelectric cut. An electrical high-frequency signal is applied to

the electrodes which generate BAWs. These sensors are also known as TSM sensors since QCMs are used as resonators in a pure thickness-shear mode. QCMs with fundamental frequencies up to 150 MHz are available with a thick substrate (0.5-1mm) and large surface area (>1 $cm^2$).

### 2.2.2 Thin-Film Thickness-Mode Sensors

Thin film thickness-mode sensors are BAW based on thickness-mode waves that are of the longitudinal type. They are also known as film bulk acoustic resonator (FBAR) sensors that are made of piezoelectric thin films. These sensors have a silicon substrate with a tiny membrane inside that vibrates (Penza et al., 2008).

Films of piezoelectric materials, such as AlN or ZnO, are created as diaphragms defined by photolithography and etched from a silicon substrate. Therefore, a high mass sensitivity and extremely thin layer with a resonance frequency of up to 1000 MHz are achievable. Although the very high working frequencies (in the range of 1–10 GHz) might provide substantial challenges to the readout electronic circuits and instrumentation, shear-mode FBARs are considered to offer a high potential, especially for fully integrated biological sensor arrays. The working frequency range for FBAR biosensors is 1000-5200 MHz, which is a very high frequency compared to other acoustic biosensors. Because of its high sensitivity, Xu et al. (2011) used the FBAR based on ZnO as piezoelectric material, they created an FBAR biosensor with a minimum detectable mass of 1.35 $ng/cm^2$ that is characterized in liquids for the real-time monitoring of protein adsorption. FBAR has a less complex structure, smaller device size, and lower manufacturing cost compared to quartz crystal microbalance (QCM) (Xu et al., 2011).

### 2.2.3 Capacitive Micromachined Ultrasonic Transducer (CMUT)

A CMUT is a MEMS device composed of two parallel plates, one is fixed (the substrate) and the other is a flexible membrane. CMUT is used to transmit and receive acoustic signals, as shown in Fig.2.1 when the membrane is vibrated by an acoustic wave, a change of capacitance can be detected and when a voltage is applied between the membrane and the substrate, it causes vibrations on the membrane which send an acoustic signal.The resonance frequency of the membrane depends on its mass and thickness, to increase the sensitivity a lower structure mass and a higher resonance frequency is needed.

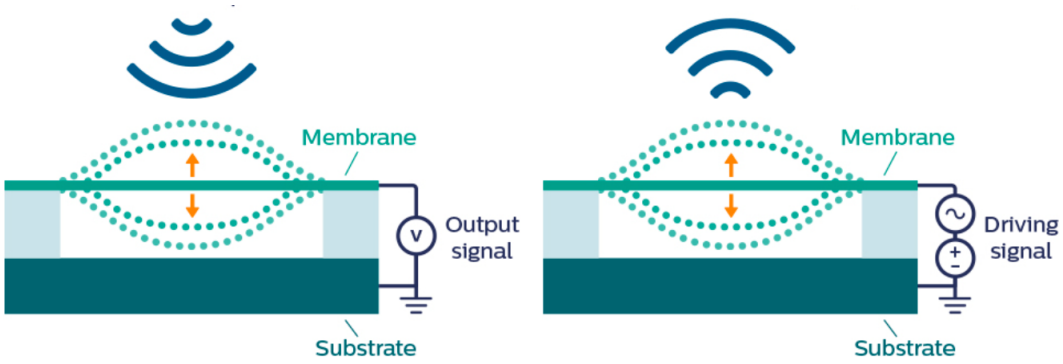


**Figure 2.1** – One CMUT cell Schematic while receiving and transmitting signal.Khuri-Yakub et al. (2007)

To make a CMUT based sensor, many cells are used which improve the accuracy. CMUT's membrane have a small mass and it works in a frequency range about tens of MHz. Eq.2.1 shows the relation between mass loading and frequency shift in a CMUT design(Khuri-Yakub et al., 2007).

$$\frac{\Delta f}{f_0} \approx \frac{1}{2}\frac{\Delta m}{m} \tag{2.1}$$

which $\Delta f$ is the shift in frequency, $f_0$ is the resonance frequency, $\Delta m$ is the amount of mass loaded and $m$ is the mass before the increase.

### 2.2.4 Piezoelectric Micromachined Ultrasonic Transducer (PMUT)

The structure of a PMUT based sensor is similar to the CMUT. A piezoelectric material is used as the membrane plate in the PMUT design. In this case, the space between two plates is not for a voltage application, it is just for the device which operates in a flexural mode to have enough place to vibrate Fig.2.2. PMUT have a unimorph structure which means that it consists of one active layer (piezoelectric layer) and one inactive layer (silicon substrate) (Qiu et al., 2015). In contrast to unimorph structures, there is a biomorph structure in which, the silicon is sandwiched between two piezoelectric layers (Horsley et al., 2015).

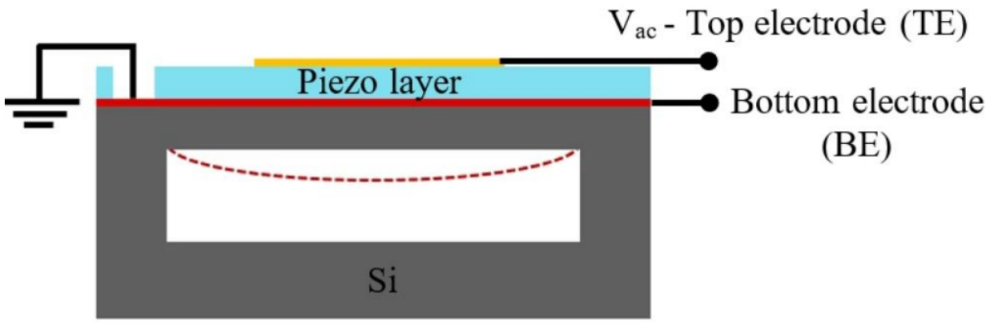


**Figure 2.2** – PMUT's schematic by Sridhar (2020)

.

### 2.2.5 Surface Acoustic Wave (SAW)

Surface acoustic waves (SAW) are mostly used for mass sensing because of their ability to confine the wave's energy on the surface (Fu et al., 2017). The wave is propagating in about one wavelength from the surface which makes the sensitivity of the SAW devices higher compared to QCM. An essential part of SAW devices is their electrodes called Interdigital transducers (IDT) which are situated on both ends of the piezoelectric material surface. A shear horizontal Wave ($SH-W$) is a kind of SAW with a lower phase velocity than that of bulk shear waves. In $SH-W$, particle displacement has a very shallow depth of penetration, therefore when $SH-W$ mode is dominant in a device, it can operate in liquids without significant radiation losses but waves with particle displacement perpendicular to the device surface have the radiation loss problem in liquids which leads to significant propagation losses (Arnau et al., 2004). Optimization of crystal cut, materials, IDT design, and oscillator electronics is required to have a dominant $SH-W$ mode. There is a method examined by Cole et al. (2004a) in $SH-W$ which conserve mechanical effects and eliminate electrical one for a liquid propagating on the delay line. In this method, there are two microsensors as shown in Fig.2.3 which, one of them is electrically shorted surface (metallized and electrically shielded) and the other remains electrically active ; the electric potential for the metallized one is zero. The approach described enables the simultaneous evaluation of the mechanical (acoustic) properties and electrical (electroacoustic) parameters of the liquid being tested. This method is usable for detecting mechanical properties of a liquid such as viscosity and electrical properties such as permittivity and conductivity(Cole et al., 2004b).

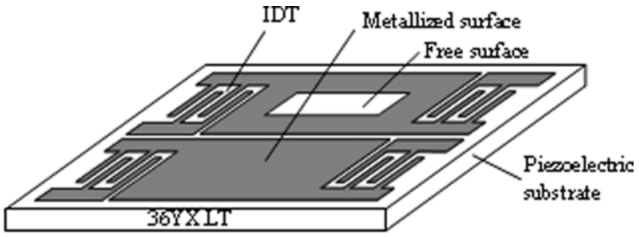


**Figure 2.3** – Schematic of a dual delay-line SH-SAW microsensor.Cole et al. (2004a)

#### 2.2.5.1 Love wave

Love wave is a shear horizontal SAW which propagates close to the surface like a snake without any vertical displacement. This biosensor's resonant frequency varies between 30 and 1500 MHz. Love wave-based microsensors have a thick substrate that creates the wave between the piezoelectric substrate and, a waveguide (guiding layer) which confines vibrations near the surface. The wave energy is confined near the surface because of the difference in mechanical properties between the substrate and the guiding layer which entraps the acoustic energy in the waveguide and slows down the wave propagation velocity. Therefore, it has a high mass sensitivity. The guiding layer plays an important role in the Love wave devices sensitivity ; the higher the wave confinement, the higher the sensitivity ; it also protects and insulates IDTs from the liquid media and reduces the risk of liquid penetration between the IDTs and resonator which is a challenge (Voinova, 2009). Different guiding layers have been tested, such as sputtered silica, SU-8 resist, polymers, ZnO, and $SiO_2$. Mass sensitivity of a Love wave device has been compared for $LiTaO_3$ substrate with two different guiding layers ; the sensitivity is higher with ZnO as the guiding layer than it is with $SiO_2$ (Powell et al., 2004b). One of the most used materials as guiding layer is PMMA because of several appropriate properties which two of them are the ability to be easily spread with a

uniform thickness by a spin-coater and a low shear velocity (1105 m/s) resulting in better wave confinement. The guiding layer needs to have a low density and low acoustic absorption in addition to the lower shear velocity discussed above. The higher the guiding layer thickness the higher the acoustic absorption which leads to a higher insertion loss. Table.2.1 shows some properties of different guiding layers.

**Table 2.1** – Properties of different guiding layers (Rocha et al., 2013).

| Guiding layer material | $\mu_L$ (GPa) | $\rho_L$ $(kg/m^3)$ | $v_L$ (m/s) |
|---|---|---|---|
| $SiO_2$ | 17.87 | 2200 | 2850.04 |
| ZnO | 40.17 | 5720 | 2650.00 |
| Au | 28.50 | 19300 | 1215.19 |
| Polyimide | 0.87 | 1420 | 780.48 |
| PMMA | 1.70 | 1180 | 1200.28 |
| PDMS | $250 \times 10^{-}6$ | 965 | 16.09 |

In order to generate this wave, a specific cut is required for the piezoelectric material (Chen et al., 2020). It is not straightforward to design a Love wave resonator that operates at a specific frequency (Rocha et al., 2013) ; there are some conditions for the existence of Love wave modes ; First, shear velocity of the overlay material should be less than that of the substrate :

$$v_L = \sqrt{\frac{\mu_L}{\rho_L}} < v_S = \sqrt{\frac{\mu_S}{\rho_S}} \tag{2.2}$$

where $v_L$ and $v_S$ are waveguide and substrate's shear velocity, $\mu_L$ and $\mu_S$ are

their shear modulus and $\rho_L$ and $\rho_S$ are their density. Second, the wavelength of the shear wave should be more than the thickness of the guiding layer. Third, the piezoelectric should have appropriate material parameters, for example, some piezoelectric material should have a specific cut to support this wave, these are two piezoelectric materials which are highly used to generate the right Love waveform : 36° $Y$–$X$ $LiTaO_3$ and 64° $Y$–$X$ $LiNbO_3$ (Rocha-Gaso et al., 2009b). $LiTaO_3$ and $LiNbO_3$ have a dielectric constant close to the water dielectric constant which lessens the mismatch effect of the dielectric constant (Arnau et al., 2004). The sensitivity of these sensors is determined by the degree of wave confinement. Qian et al. (2018) have demonstrated the effect of different crystal cut on waves mode in a SAW device.Luo et al. (2013) developed a glucose biosensor with a multilayer Love mode surface acoustic wave. They reached a sensitivity of 7.184 MHz/mM and an accuracy of 6.96 $10^9$ mM. Song et al. (2011) developed a wireless Love wave device that can detect two different particles with a single device. Compared to SAW which don't have a guiding layer, Love wave's mass sensitivity is increased by more than two orders of magnitude, and the SAW substrate is about 100 times thicker than Lamb Wave's, which affects the whole device's size. One other type of SAW is Rayleigh waves which its deference with Love wave can be seen in Fig.2.4

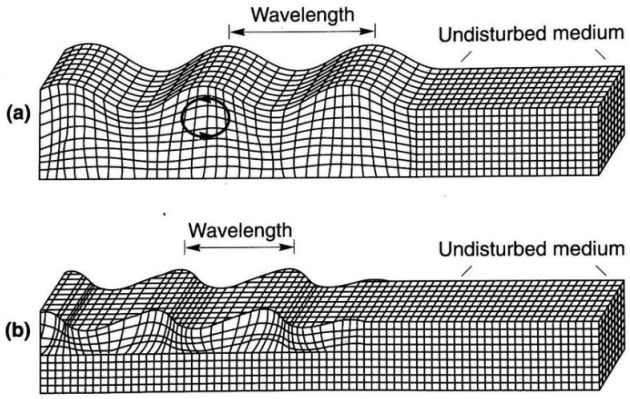


**Figure 2.4** – Illustration of surface wave motion. Rayleigh wave (a) and Love wave (b)(Shoushtari, 2016)

It has good sensitivity but compared to the Love wave ; it is less sensitive because of the energy loss for the vertical displacement. There is also a signal attenuation because of a dielectric mismatch between the liquid and the substrate which attenuates the output signal. Love wave device fabrication (Lai, 2015) :

— Two important factor for love wave creation are the piezoelectric substrate and the guiding layer.

— Aluminum at a thickness of around 150 nm is deposited using a thermal evaporator.

— The photoresist (PR) is spin-coated for the IDT.

— Photo resist is exposed to the UV light with the IDT pattern.

— The aluminum is wet etched.

— PMMA is spin-coated at a thickness around 0.7 m and then cured at

— 180 C for 2 h to remove all solvent and improve adhesion of the PMMA waveguide layer onto the substrate.

### 2.2.6 Lamb wave

Lamb wave is a kind of BAW, it is an elastic wave that propagates along a thin layer membrane. Fig.2.5 shows how each of the two modes of this wave is propagating in the resonator.

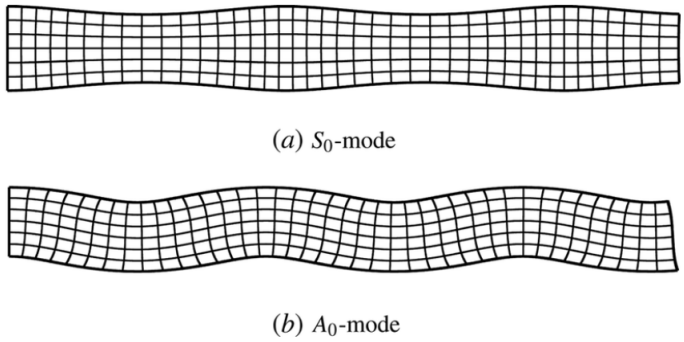


**Figure 2.5** – Lamb wave mode shapes for a) S0 mode, b) A0 mode.(Willberg et al., 2015)

For a specific wavelength, the resonance frequency is comparatively low (5-20 MHz), reducing electronics requirements. To have a lamb wave, the membrane thickness should be smaller or equivalent to the wavelength. Lamb wave velocity is defined by the waveguide's material, and $h/\lambda$ ratio, in which h is the piezoelectric thickness and $\lambda$ is the acoustic wavelength. Both symmetric and antisymmetric modes can be generated in a Lamb wave device. Our concern is the A0 mode, often called flexural plate waves (FPWs), which refers to the antisymmetric mode. The S0 mode, also called extensional mode, is generated symmetrically, S0 and A0 sensitivities are the same for solid sensing but there are some differences in liquid sensing. The zero-order antisymmetric mode A0 is seen in devices operating in the range of 5 to 300 MHz and exhibits low attenuation within liquids, which is essential for biological mass sensing. Lamb Waves have demonstrated signifi-

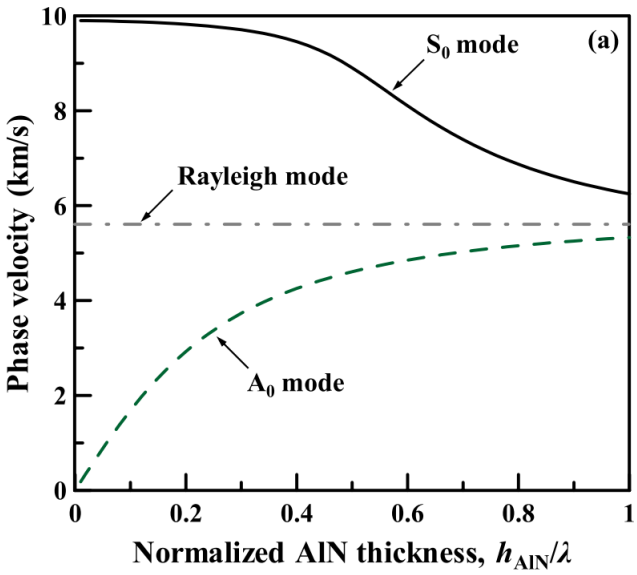


**Figure 2.6** – Velocity of the A0 and S0 Lamb wave modes traveling through the AlN membrane.(Lin et al., 2014)

cant sensitivity to mass loading, specifically for liquids which is our interest. The sensing procedure is the same for both SAW and Lamb waves, electrical sinusoidal signal is applied to input IDTs, this electrical signal is then transformed to a mechanical wave through the piezoelectric material which creates the acoustic wave. In the other side, the acoustic wave is reconverted into an electrical signal which is recorded from the output IDTs. This output sinusoidal signal is used to detect different physical and chemical properties of gas or liquids (Voinova, 2009). As you can see in Fig.2.6 by increasing the piezoelectric thickness, the A0 mode wave becomes closer to the Reighley mode which means that by increasing h, the Lamb wave resonator is transformed to a SAW resonator.

Radiation loss is one of the disadvantages of Lamb Wave devices which is reduced in our device. Lamb wave velocity can be controlled by the wavelength and the piezoelectric thickness, so a lower velocity than the sound phase velocity can be obtained which avoids high radiational losses in liquids (Weckman and Seshia,

2017).

## 2.3 Mass sensor

There are different methods to detect the mass of some liquid solutions in an acoustic microsensor. One of the usual methods is by measuring the resonance frequency of the device before and after adding the solution, the second is to detect the phase difference between the input signal and output signal. The resonant frequency of a piezoelectric resonator is influenced by the mass change on the surface of this resonator. When a particle is attached to the sensing area, a resonance frequency shift occurs on the device, this frequency shift determines the amount of mass variation by using this formula (Mujahid and Dickert, 2017) :

$$\Delta f = -\frac{k\Delta m f_s^2}{A} \tag{2.3}$$

Where $\Delta f$ is the resonant frequency shift (Hz), $\Delta m$ is the mass variation(g), $K$ is the constant value for the piezoelectric material, $f_s$ is the fundamental frequency and A is the absorbing surface area ($cm^2$).

### 2.3.1 Immobilisation

One challenging part of mass sensing is the way that particles stick to the device's surface. One of the methods to identify a specific particle is using the antibody-antigen interaction, this is similar to a lock and key fit where the antigen binds to the antibody only if it has the correct conformation (Parizi et al., 2022). An antigen is a molecule such as bacteria, viruses, fungi, allergens, venom, and other

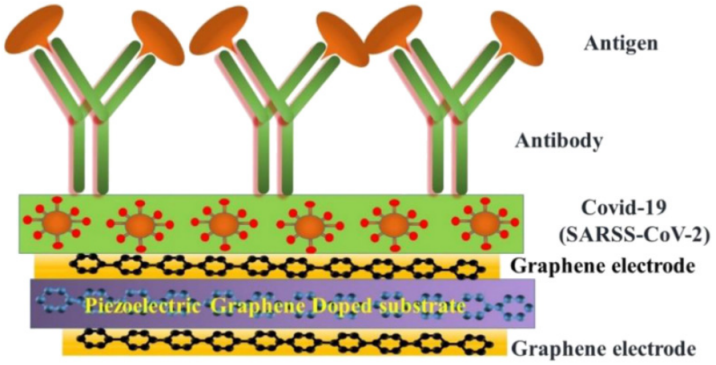


**Figure 2.7** – Coronavirus absorption using piezoelectric graphene.(Srivastava et al., 2020)

various toxins that enters your body and is able to stimulate an immune response(Guisan et al., 2006). An antibody is a protein that is produced by the immune system to stick to antigens as Fig.2.7 and fight them(Guisan et al., 2006).

Therefore, to detect specific bacteria, viruses, and any other toxins in a liquid, the corresponding antibody is needed. Antibodies also must be immobilized with a material such as carbon allotropes, a specific protein, and gold for its adhesion and non-reactivity (Kumar et al., 2000). There are various methods of immobilization which are explained in detail in (Guisan et al., 2006). One of those is the immobilization by carbon allotropes, as shown in Fig.2.7. Graphene is an allotrope of carbon in which every atom is available for a chemical reaction from two sides. Chang and Shih (2007) developed a SAW biosensor based on fullerene (C60) which is also one of the carbon's allotropes, they immobilized C60-enzymes/antibodies/proteins to detect different particles. A layer of C60-hemoglobin is deposed into the piezoelectric material ($LiTaO_3$) which absorbed anti-hemoglobin (Chang and Shih, 2007). Kumar et al. (2000) described the construction of an antibody-based piezoelectric sensor capable of detecting mycobacterial antigen in diluted cultures of attenuated.

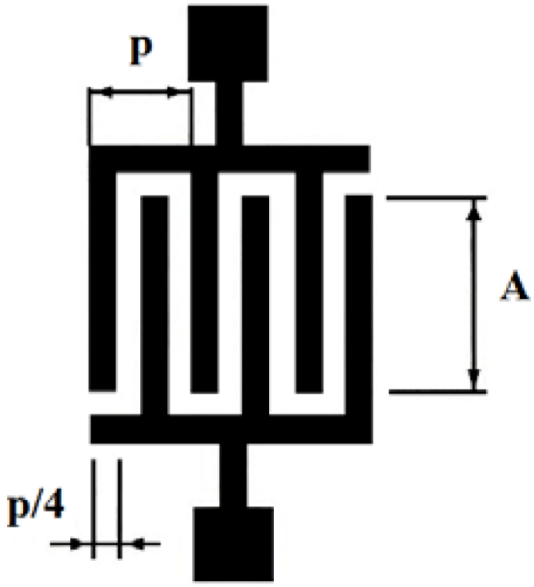


**Figure 2.8** – IDTs with period p.(Rocha-Gaso et al., 2009a)

## 2.4 Interdigital transducer

IDT is an electrode that when AC voltage is applied to, acoustic wave is generated in the piezoelectric substrate and vice versa. In a love wave sensor, IDTs are sandwiched between the piezoelectric substrate and the guiding layer.There are transmitter and receiver IDTs in a two-port acoustic microsensor and the space between transmitter IDTs and receivers is called the delay line. The longer the delay line is, the lower is the transmission gain. The acoustic wave propagates along the axis perpendicular to the fingers in both directions. IDTs are mostly rectangular like what you can see in Fig.2.8, but they can also have different shapes and dimensions. The acoustic wave's wavelength is defined by the space between IDTs, as you can see in Fig.2.8, P=$\lambda/2$ where P is IDT's finger pitch.

When SAWs arrive at the IDT, if the period of the IDTs and SAW match, an electrical signal is generated between the IDT electrodes (Agache et al., 2011). As

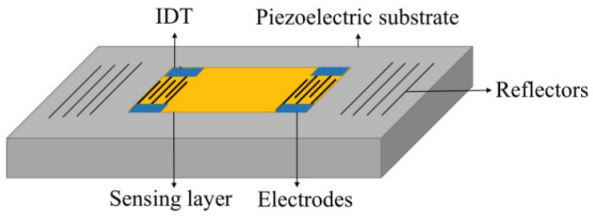


**Figure 2.9** – SAW gas sensor schematic with two reflector arrays.(Nazemi et al., 2019)

$f{=}v/\lambda$, for SAWs, the central frequency of the device is defined by the materials which characterize the velocity of the wave and the IDT period which designate the wavelength. Reflectors which are shown in Fig.2.9 are similare to IDTs with no signal connected, their role is to reflect the acoustic energy to the IDTs to reduce the dissipation of energy Nazemi et al. (2019).

Two important factors that are essential for IDTs are their shape and the way that the signal is applied to them. As shown in Fig.2.10 the input signal can be applied in different ways, in the usual method, IDTs are alternatively connected to the sinusoidal signal, and ground. Other ways are applied by adding an electrode on the bottom of the resonator, this electrode can be connected to the ground or be floated (Lin et al., 2014), in Fig.2.10, equivalent circuits for each of discussed models are shown.

As you can see, Lin et al. (2014) provided the equivalent circuit model for each of these different methods of applying signal. They conclude that when the bottom electrode is grounded, the static capacitance is higher than when they have a floating bottom, and the coupling coefficient is increased. Physical characteristics of IDTs such as IDT width, metallization ratio, number of IDTs affect a lot the device's properties. The higher the number of IDT fingers is, the narrower is the frequency response of the sensor, this increase in the number of IDTs pair will also affect the scattering and the losses which are influenced by the mass loading

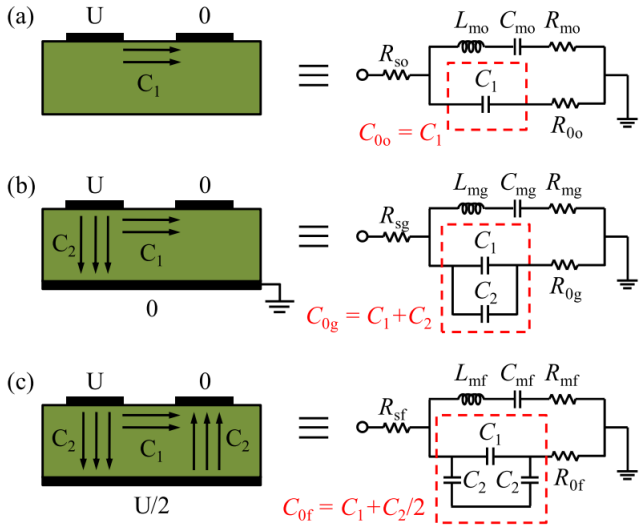


**Figure 2.10** – Equivalent circuits for the resonators with the electrically (a) open, (b) grounded, and (c) floating bottom surface topologies.(Lin et al., 2014)

(Rocha et al., 2013). The effect of the metallization ratio on the transmission gain, THD and, sensitivity is investigated in chapter 3.

## 2.5 Layer thickness

There is an optimal thickness for each layer to achieve the optimum sensitivity, the important ratio is $h/\lambda$ which h is the whole device thickness for Lamb wave devices but for Love waves it refers to the guiding layer. The $h/\lambda$ variation affects the sensitivity of the biosensor. In Fig.2.6 the diagram of three different modes are shown, as shown in this figure, their phase velocity depends to $h$ and $\lambda$, higher the $h/\lambda$ for an AlN membrane, higher is the lamb wave's velocity, until when $h = \lambda$, at this point, the lamb wave mode is transformed into a rayleigh mode which is a SAW (Lin et al., 2014). Based on Fig. 2.6, for a lamb wave, the velocity is approximately linear an equal to $f\lambda$ for $h \ll \lambda$. The thickness, mechanical characteristics, and boundary conditions of the conducting composite

plate all affect the Lamb wave's velocity. This simple asymptotic equation can accurately approximate the phase velocity of the thin-plate (Yu and Tsai) :

$$v_p = \sqrt{\frac{B + T_x}{M}} \tag{2.4}$$

where M is the mass per unit area of the plate, Tx is the component of in-plane tension in the propagation direction, and B is the bending stiffness of a homogeneous, elastically isotropic plate. The bending stiffness for an A0 mode lamb wave in a tension-free plate is (Yu and Tsai) :

$$B = (\frac{\lambda}{2\pi})^2 \frac{E'h^3}{12} \tag{2.5}$$

where $E'$ is the effective Young's modulus :

$$E' = \frac{E}{1 - v^2} \tag{2.6}$$

where E is the Young's modulus and v is the Poisson's ratio of the material.

Trivedi and Nemade (2015) have simulated different guiding layers for a love wave biosensor, they investigated the acoustic wave velocity, coupling coefficient, and device's sensitivity for $SiO_2$, ZnO, gold, SU-8, and parylene-C as guiding layer with $h$ and $h/\lambda$ variation.

## 2.6 Comparison

In this study, we first reviewed several acoustic biosensors and identified all their benefits and disadvantages. Our objective was to choose one of these biosensors, optimize it, and use it to investigate some novel ideas. We were looking for an acoustic biosensor with a competitive sensitivity, less noise, the ability to operate in liquid solutions, compatibility with CMOS technology, and the potential to be commercially accessible. Lamb wave biosensors were chosen because they possessed all of the above-described qualities that were significant to us. What follows explains the raisons for our decision.

**QCM :** When used for liquid sensing, the QCM biosensor's performance declines as a result of the fluid sample interfering with signal transduction, therefore this biosensor was not the ideal option for us because we were looking for a sensitive biosensor that works well in liquid environment. Also, our interest was to find a sensitive mass detector, but we found that QCM biosensors have low mass detection limits due to their low operating frequency (5-30 MHz). This biosensor is incompatible with CMOS processing which was important for us (Nair et al., 2021).

**FBAR :** FBAR limitations are Poor anti-interference performance, Hard measurement because of the noises, and Fragile membrane (Zhang et al., 2021a). The main reason that we skipped this biosensor was limitations related to the fabrication such as the difficulty of manufacturing the fragile free-standing structures, its longer fabrication time and the absence of large scale commercialization (Nair et al., 2021).

**CMUT & PMUT :** CMUTs are mostly used for diagnostic imaging, due to temperature restrictions imposed by the existing metal lines on the electronics,

processing techniques for producing CMUTs are still limited (Khuri-Yakub and Oralkan, 2011). In comparison to other biosensors discussed, the PMUT's average operating frequency is low ; it ranges from 100 KHz to 1300 KHz, which restricts the ability for mass detection (Ahmad et al., 2017).

**Love wave :** Because of its high sensitivity, we initially decided to use the Love wave device to test our new ideas and perform the necessary simulations for this type of wave, but, subsequently, we found that SilTerra's commercial CMOS technology is rather suitable for use as a lamb wave device. Additionally, Love wave device fabrication is more difficult because we would have had to complete the entire fabrication process in our lab and it is challenging to excite a pure shear mode on the device's surface, which makes it challenging to produce a Love wave. Therefore, we ultimately selected the Lamb wave instead (Nair et al., 2021).

**Lamb wave :** The potential to be commercially available was the key factor in why Lamb wave biosensors were more suited for our research than the others. In order to create a microelectromechanical system (MEMS) with existing commercial technology, we employed SilTerra's CMOS technology properties in our simulations, including materials, layer thicknesses, and other measurements. In addition, they belong to the group of highly sensitive biosensors that can easily operate in liquid media (Nair et al., 2021).

CHAPTER III

# A STUDY OF OPTIMIZING LAMB WAVE ACOUSTIC MASS SENSOR PERFORMANCE THROUGH ADJUSTMENT OF THE TRANSDUCTION ELECTRODE METALLIZATION RATIO.

The design and simulation work was done by me.

Prof. Cicek, Prof.Robichaud and Prof.Shih had a role of theoretical support, discussion of results and revision of the manuscript.

Fatemeh Gholami , Andy Shih , Alexandre Robichaud and Paul-Vahe Cicek *

## ABSTRACT

This paper presents the design and simulation of a mass sensitive Lamb wave microsensor with CMOS technology provided by SilTerra. In this work, the effects of the metalization ratio variation on the transmission gain, total harmonic distortion (THD), and two different resonant modes (around 66 MHz and 86 MHz) are shown. It has been found that the metalization ratio can be adjusted in order to obtain a compromise between transmission gain and sensitivity, depending on the design criteria. By adding a $Si_3N_4$ layer on top of the device, a five-fold improvement in transmission gain is reached. It was also shown that the transmission of the input differential IDT configuration is 20% more efficient than a single

terminal. With this combination, the mass sensitivity is about 114 [$cm^2$/gr].

keyword :lamb wave ; mass sensing ; microsensor ; metalization ratio ; CMOS ; THD ; acoustic microsensor.

## 3.1 Introduction

With ongoing improvements in microfabrication technologies, acoustic microsensors are becoming increasingly attractive for physical or chemical measurements within liquid and gas environments, such as relative humidity (Hong and Chung, 2010), temperature (Lee et al., 2022), pH (Piro et al., 2021), and pressure (Choujaa et al., 1995). Cell detection and analysis is also a target of great interest within microfluidic systems Zhan et al. (2022) ; Sakaguchi et al. (2022) ; Oda et al. (2021) ; Akiyama (2021). In particular, acoustic mass sensing is a proven method to detect various chemical or biological analytes, and as such, can play a significant role in medical diagnosis (Fu et al., 2017 ; Zhang et al., 2021b). For instance, Chang et al. used an acoustic microsensor for insulin detection, allowing the subsequent use of glycine-HCL to remove insulin for further testing (Chang and Shih, 2007). Luo et al. developed a glucose biosensor using a multilayer Love-mode surface acoustic wave, achieving a sensitivity of 7.184 MHz/mM and an accuracy of $6.96 \times 10^{-3}$ mM (Luo et al., 2013). Moreover, acoustic sensors have been used to detect different DNA (Trivedi and Nemade, 2015) and cancer cells (Tigli et al., 2010). Tigli et al. developed a surface acoustic wave (SAW) device using a gold layer to immobilize specific antibodies on its surface in order to detect a specific antigen that is a cancer biomarker (Tigli et al., 2010). Another application of mass sensing devices is to determine water quality by measuring and characterizing pH ; biochemical oxygen demand ; total organic carbon ; and nitrate, nitrite, ammonia, chlorine, and fluoride concentrations (Tamarin et al., 2020 ; wat, 2011). Tamarind

et al. presented a surface acoustic wave microfluidic chip with the ability to assess water quality on-site (Tamarin et al., 2020).

Acoustic microsensors are operated by applying an electrical signal to input interdigital electrodes (IDTs) situated on a piezoelectric material. The piezoelectric material transforms the electrical signal into mechanical waves (Pohanka, 2018), which travel within the substrate. At a certain distance from the input, output IDTs reconvert the mechanical waves into an electrical signal, but with a phase difference according to the distance traveled and the physical properties of the medium. Any mass added onto the piezoelectric sensing area between the input and output IDT will result in a proportional variation in the phase difference between input and output signals.

In order to detect the presence of an analyte within a liquid solution through mass sensing, immobilization must be achieved so as to selectively isolate the specific component of interest. In the context of biological sensing, where detection of an antigen is often of interest, antibodies can be affixed at the sensing zone using graphene (Hossain and Shimizu, 2019), gold nanoparticles (Huang et al., 2015; Tang et al., 2004; Pantazis et al., 2014), or other suitable materials that are effective at retaining the specific antibody. When an antigen particle becomes attached to the immobilized antibodies on the sensing area, the variation in mass affects the resonance frequency of the sensor. This phenomenon can be harnessed to infer the amount of analyte that is circulating (Aslam et al., 2020).

A critical factor in mass-sensitive acoustic devices is IDT geometry. The length, width, number, and shape of IDTs affect device behavior (Fu et al., 2010). Skinner et al. studied the effect of IDT width on the efficiency of energy conversion of a SAW device (Skinner et al., 2006). Kuznetsova et al. (2020) evaluated the impacts of IDT finger length on acoustic plate wave synthesis. There are also

various configurations for applying actuation voltage to the IDT, leading to various electrical field distributions on the device. Zou et al. studied the effects of different electrode materials, transducer configurations, and electrode thicknesses on the coupling factor in an aluminum nitride (AlN) lamb wave resonator using the symmetric mode. As a result, they found a better coupling factor when using transducers on both sides of the piezoelectric device (Zou et al., 2017).

Acoustic microsensors can rely on different types of acoustic waves to measure or detect the presence of biological particles. For example, a lamb wave, which exhibits significant sensitivity to mass loading specifically within liquids (Caliendo and Hamidullah, 2019), is an elastic wave that propagates along a thin layer membrane, whose thickness is less than or equivalent to the wavelength at play (Fu et al., 2017; Wenzel and White, 1988). Kong et al. developed a lamb wave sensor to assess blood clot formation, in order to predict the risk of cardiovascular disease (Kong et al., 2019). Lamb wave sensors can also be used for the detection of microparticles. Nam et al. implemented a lamb wave sensor that can detect the presence of nucleic acids in less than 30 min (Nam et al., 2019). Lamb wave detection has been successfully demonstrated in environmental sensing applications such as humidity (Kuznetsova et al., 2017), temperature (Yule et al., 2021), and pressure (Caliendo and Hamidullah, 2018) monitoring.

There are two main approaches for implementing these acoustic sensors. They can either be fabricated on a piezoelectric substrate to interface with a distinct electronic circuit or be integrated monolithically with complementary metal–oxide–semiconductor (CMOS) technology. With CMOS monolithic integration, the direct inclusion of integrated electronic circuits renders the whole system smaller and more compact, reduces parasitic capacitance, and has the potential to significantly lower costs at scale. Furthermore, assembly and packaging are simplified by eliminating the need for combining several heterogeneous chips with complex

mounting or wirebonding schemes. References Salim et al. (2017) ; Zhang et al. (2015) ; Kishor et al. (2016) present examples of heterogeneous sensor implementations. Tigli et al. implemented a CMOS integrated SAW device with a ZnO piezoelectric membrane for cancer biomarker detection with a frequency sensitivity of 8.704 pg/Hz (Tigli et al., 2010). In this paper, we propose a mass sensitive lamb wave microsensor designed with dual interdigital electrodes (IDT) for biological mass sensing, which can be integrated monolithically with CMOS SilTerra technology and its $Si_3N_4$ layer, which provides a fivefold improvement in transmission gain. The technology, aside from the inherent benefits provided by monolithic integration, features a very thin suspended piezoelectric layer of aluminum nitride (AlN), which promises superior sensitivity compared to thicker ones (Duhamel et al., 2006). Furthermore, the top layer of silicon nitride ($Si_3N_4$) can be utilized to protect the device from direct contact with the fluidic environment (Zamora et al., 2020), while also serving as an acoustic wave guiding layer to improving the transmission gain of the device. With the parameters of the selected technology for this work, lamb wave operation is the most appropriate with which to perform mass sensing. In order to optimize insertion loss and coupling factor, differential mode signals are investigated, and the impacts of IDT width on sensitivity and transmission gain. Total harmonic distortion (THD) is also studied to assess system linearity.

This article is divided into five sections : Section 3.2 provides a theoretical overview of lamb waves, IDTs, and the sensitivity metric ; Section 3.3 details the parameters and specifics of the proposed device, and provides an overview of the simulation methodology ; Section 3.4 presents and discusses the simulation results ; Section 3.5 concludes.

## 3.2 Theoretical Background

Lamb wave velocity is defined by the waveguide material, and the $h/\lambda$ ratio, in which $h$ is the piezoelectric layer thickness and $\lambda$ is the acoustic wavelength (Duhamel et al., 2006 ; Malik et al., 2016 ; Wingqvist et al., 2009). Both symmetric and antisymmetric modes can be generated in a lamb wave device (Fu et al., 2017). The S0 mode, also called the extensional mode, is generated symmetrically, whereas the A0 mode, associated with flexural plate waves (FPWs), is antisymmetric. S0 and A0 sensitivities are the same for solid sensing, but there are some differences in liquid sensing (Wu and Zhu, 1996). The zero-order antisymmetric mode A0 is seen in devices operating in the range of 5 to 30 MHz (Pantazis et al., 2010) and exhibits low attenuation within liquids, which is essential for biological mass sensing. The shift in resonant frequency, $\Delta f$, in response to a variation in analyte mass per unit area, $\Delta m$, can be used as a means to detect the presence and measure the quantity of the analyte.

Mass sensitivity is defined as Duhamel et al. (2006) ; Han and Yuan (2014) :

$$S_m = \frac{\Delta f}{\Delta m \cdot f_s} \tag{3.1}$$

where $f_s$ is the unloaded resonance frequency.

Radiation loss, which is a critical factor in lamb wave attenuation, is minimized in the A0 mode compared to the S0 mode, provided that its phase velocity is inferior to the velocity of a bulk acoustic wave in the liquid medium (Yantchev and Katardjiev, 2013 ; Viktrov, 1967). In the A0 mode, wave velocity can be controlled by the wavelength and the piezoelectric thickness ; thus, a phase velocity lower than the nominal velocity of sound can be obtained, decreasing radiation losses in liquids. By increasing the piezoelectric layer's thickness, the A0 and S0 mode waves converge with the Rayleigh mode (Lin et al., 2014).

Lin et al. showed that with an AlN-based symmetric mode lamb wave, by increasing $h/\lambda$ to 1, the phase velocity increases to around 5.5 km/s Lin et al. (2014). In the present work, $h$ is 1.3 µm and $\lambda$ is 20 µm, yielding a phase velocity of around 0.8 km/s, corresponding to the $h/\lambda$ vs. phase velocity curve presented by Lin et al. for the A0 mode.

IDT geometry affects certain properties of the device. IDT finger length and the number of electrodes determine electrical impedance : the lower the length, the higher the impedance Wohltjen (1984). Another important characteristic of IDT is the metalization ratio, $\eta$. It is defined as $\eta = w/p$ where $w$ is the finger width and $p$ is the pitch (center-to-center) between each finger, as shown in Figure 3.1. $\eta$ affects the coupling factor and the insertion loss Nakamura et al. (2007). The effects of $\eta$ on sensitivity, transmission gain, and THD are also investigated ; the results are presented in Section 3.3.

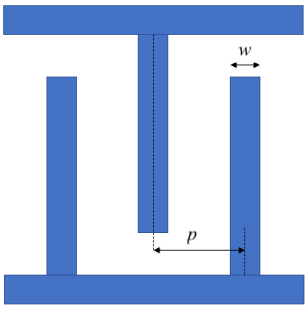


**Figure 3.1** – IDT with a metalization ratio of $w/p$.

Skinner et al. studied the impact of metalization ratio on the efficiency of energy conversion for a SAW sensor, reporting optimal output energy for $\eta$ of 0.74.

Within an acoustic waveguide, there are countless acoustic modes that can propagate Caliendo et al. (2018). Each mode has its specific shape and phase velocity ($v_p$). IDTs generate a force on the piezoelectric surface, producing a displacement

in the piezoelectric resonator, which in turn can excite acoustic wave modes Dieulesaint and Royer (1980). The mode whose displacement shape has more correlation (overlap integral Awai and Zhang (2006)) with the displacement produced by the IDT will be excited with greater power. As a result, the greater the coupling efficiency, the greater the transmission gain will be. Varying the IDT metalization ratio induces a slightly different displacement shape. Depending on the shape of a given mode, its optimal IDT metalization ratio can vary. Considering that fundamental $\lambda$ is dictated by IDT pitch, the resonant modes can appear at different frequencies as per $f = v_p/\lambda$.

In this study, the THD of the transmitted signal is also examined in order to assess the linearity of the system, or in other words, the extent to which varying the IDT metalization ratio introduces harmonic distortion. For a pure harmonic input signal at a given frequency, total harmonic distortion is defined as :

$$THD = \frac{\sqrt{V_2^2 + V_3^2 + V_4^2 + ...}}{V_1} \tag{3.2}$$

where $V_n$ is the root mean square (RMS) voltage of the $n$th harmonic of the received signal.

## 3.3 System Overview and Simulation Methodology

The two-port device developed in this work through the SilTerra technology is schematized in Figure 3.2. It consists of a thin layer of aluminum beneath 1.3 µm of aluminum nitride (AlN), the piezoelectric material, covered by 1.5 µm of $Si_3N_4$, the protection and waveguide material. The separation between the transmitter and receiver IDT acts as the delay line, enclosing the sensing area with the immobilizers that were explained in the previous section.

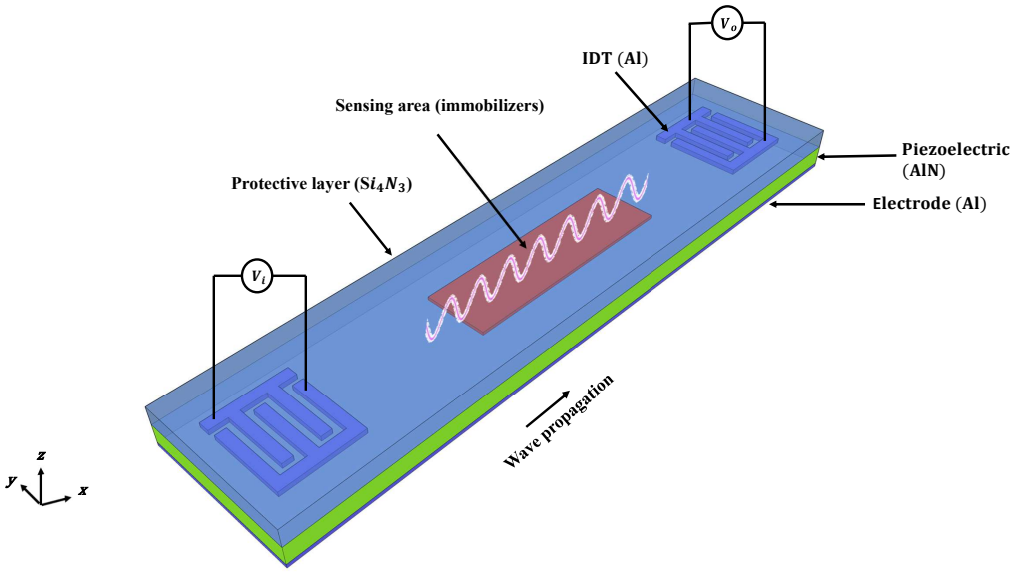


**Figure 3.2** – Three-dimensional schematic of the device showing different layer order, IDT locations, and the wave propagation direction.

The SilTerra technology provides a suspended AlN piezoelectric layer directly above a conventional 130 nm CMOS semiconductor process, as illustrated in Figure 3.3. The technology features a thin layer of AlN, which helps improve sensitivity (Duhamel et al., 2006) and a $Si_3N_4$ layer for protection and wave guiding.

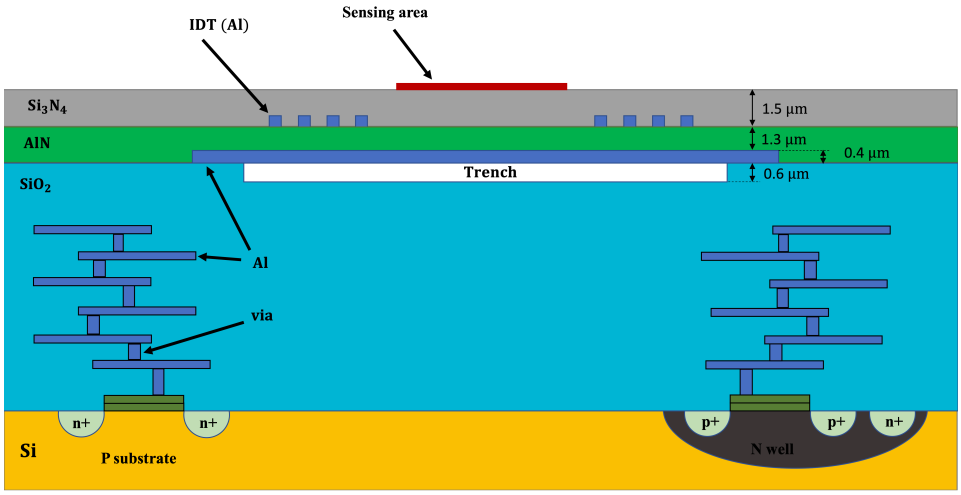


**Figure 3.3** – Cross-section of the Lamb wave microsensor realized with the CMOS Silterra technology.

In this work, COMSOL Multiphysics 6.0, Stockholm, Sweden, was used to perform finite-element method (FEM) simulations. An sinusoidal electrical signal was applied to the input IDT and transformed into mechanical waves through the piezoelectric layer (as shown in Figure 3.4, 200 ns after voltage application). The resulting induced electrical signal at the output IDT was monitored and analyzed to design a sensitive mass sensor.

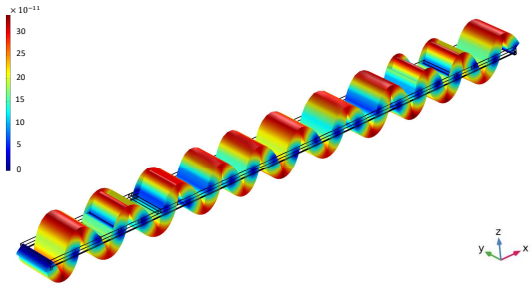


**Figure 3.4** – Time-domain simulation of the lamb wave illustrating the wave propagation and the total displacement of each part of the device at 216 ns with an input signal frequency of 86 MHz and metalization ratio of 85%.

One of the methods to detect a variation of mass in acoustic sensors is to measure the device's resonance frequency before and after mass loading. Based on (3.1), the greater the frequency shift, the greater the sensitivity (Han and Yuan, 2014). The physical properties of AlN used in the simulation are listed in Table 3.1.

**Table 3.1** – AlN physical properties used in this work's simulations (Zou et al., 2017).

| | **Symbol** | **AlN** | **Unit** |
|---|---|---|---|
| Stiffness constants | $C_{11}$ | 345 | $10^9$ [N/m$^2$] |
| | $C_{12}$ | 125 | |
| | $C_{13}$ | 120 | |
| | $C_{33}$ | 395 | |
| | $C_{44}$ | 118 | |
| | $C_{66}$ | 110 | |
| Dielectric constants | $\varepsilon_{11}$ | 8.0 | $10^{-11}$ [F/N] |
| | $\varepsilon_{33}$ | 9.5 | |
| Piezo constants | $e_{15}$ | $-0.48$ | [C/m$^2$] |
| | $e_{31}$ | $-0.58$ | |
| | $e_{33}$ | 1.55 | |
| Mass density | $\rho$ | 3260 | [Kg/m$^3$] |

All FEM simulations were performed using COMSOL Multiphysics and analyzed in Mathworks MATLAB R2022a, Natick, MA, USA. Importantly, all layer physical properties and dimensions followed the specifications, guidelines, and design rules of the SilTerra technology, in order to ensure that the CMOS-compatible acoustic sensor design would be implementable. The input IDTs were defined as terminals with a sinusoidal signal of $5\sin(2\pi f_r t)$. In order to choose the excitation frequency $f_r$, a frequency study was first performed to determine the resonance frequency peaks for the design under consideration, as shown in Figure 3.5. The wave modes corresponding to these resonance frequency peaks were determined by analyzing their respective wave deformation shapes. It can be observed that the localization of the dominant frequency peak changes when the metalization ratio passes about 50%. For a metalization ratio superior or equal to 50%, the dominant frequency

is located at 86 MHz and is labeled *mode a*. For a metalization ratio inferior to 50 %, the dominant frequency peak is located at 66 MHz and is labeled *mode b*. Both a and b modes behave similarly to A0 lamb waves but for different phase velocities. The phase velocity for *mode a* at a metalization ratio of 85 % was determined to be 2.013 km/s, whereas it was found to be 1.672 km/s for *mode b* at a metalization ratio of 40 %. It is posited that the existence of these two A0-like modes can be explained by the varying mode shape deformations induced by the different metalization ratios.

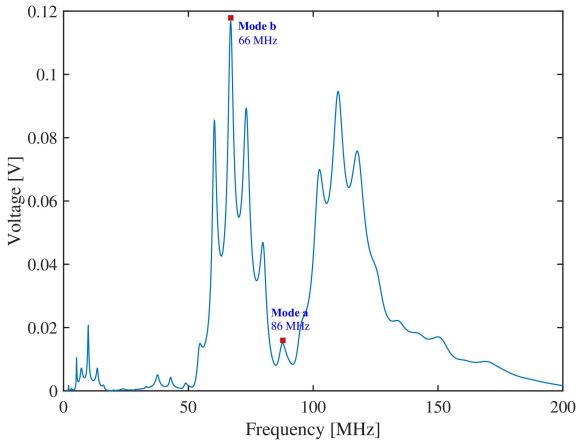


**(a)**

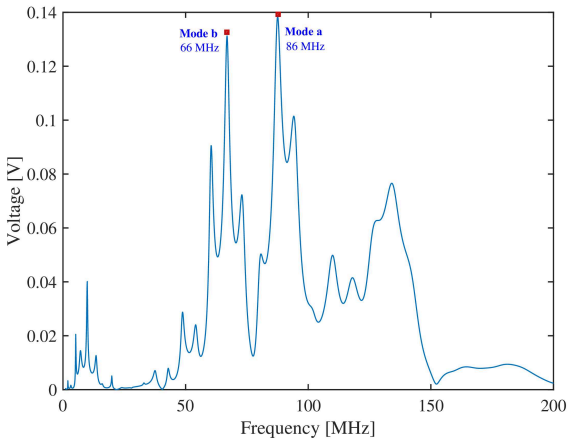


**(b)**

**Figure 3.5** – *Cont.*

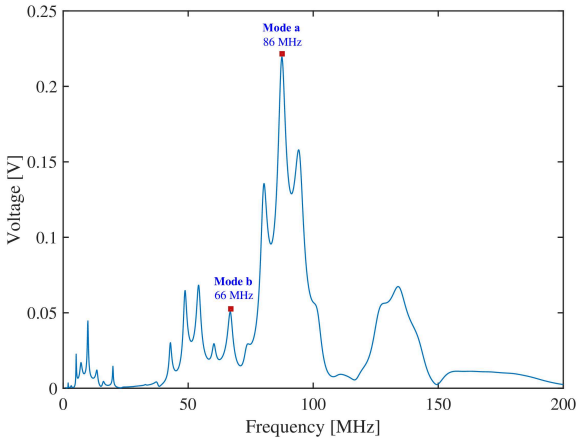


**(c)**

**Figure 3.5** – Mode a and mode b shown in output frequency spectrum for metalization ratios of (**a**) 10%, (**b**) 50%, and (**c**) 85%.

In order to configure the simulation model to accurately represent reality, two periodic boundary conditions are used on both ends of the device parallel to wave propagation, along with low reflecting boundaries for both ends orthogonal to wave propagation, in order to eliminate any unrepresentative wave reflections that might behave destructively. As shown in Figure 3.6, it takes about 40 ns for the acoustic signal to reach the output IDT, but about 350 ns for it to stabilize. To assess mass sensitivity in COMSOL without varying other device conditions, a thin layer of immobilizer PMMA is placed above the $Si_3N_4$. To simulate the loading of additional mass, the density of the PMMA is correspondingly increased. Any increase in mass density affects the velocity of the lamb wave and alters the resonance frequency and phase shift of the device. As a result, mass sensitivity can be inferred.

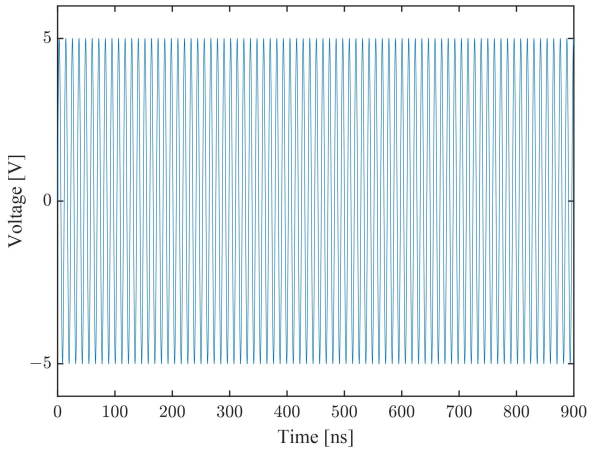


**(a)**

**Figure 3.6** – *Cont.*

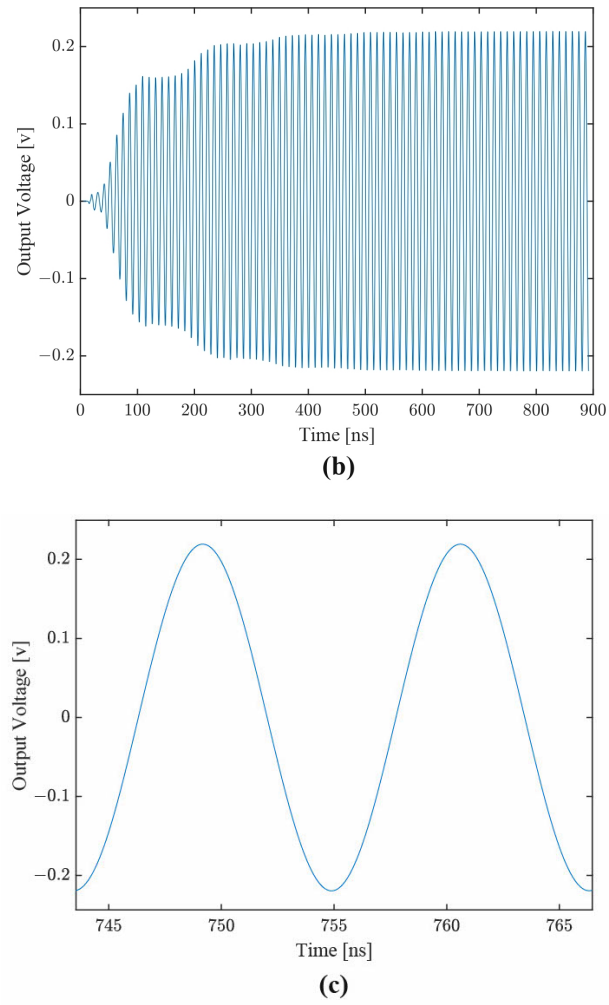


**Figure 3.6** – Time domain simulation waveforms for IDT metalization ratio of 85% : (**a**) harmonic signal with amplitude of 5 V applied to input IDT starting at time t = 0 ; (**b**) received signal at output IDT ; (**c**) close-up of two periods of received signal from 745 to 765 ns.

The use of a technology providing monolithic integration of acoustic and CMOS semiconductor devices creates the possibility of a full chip-scale system, such as the one suggested in Figure 3.7. In this setup, a harmonic signal is generated at a specific frequency, as defined by the digital signal processing (DSP) unit, then amplified and fed to the input IDT. A harmonic signal at the same frequency is

received and amplified at the output IDT, digitized, and processed by the DSP. By sweeping the excitation frequency, DSP can determine the system's resonance frequency, hence the deposited mass on the sensor.

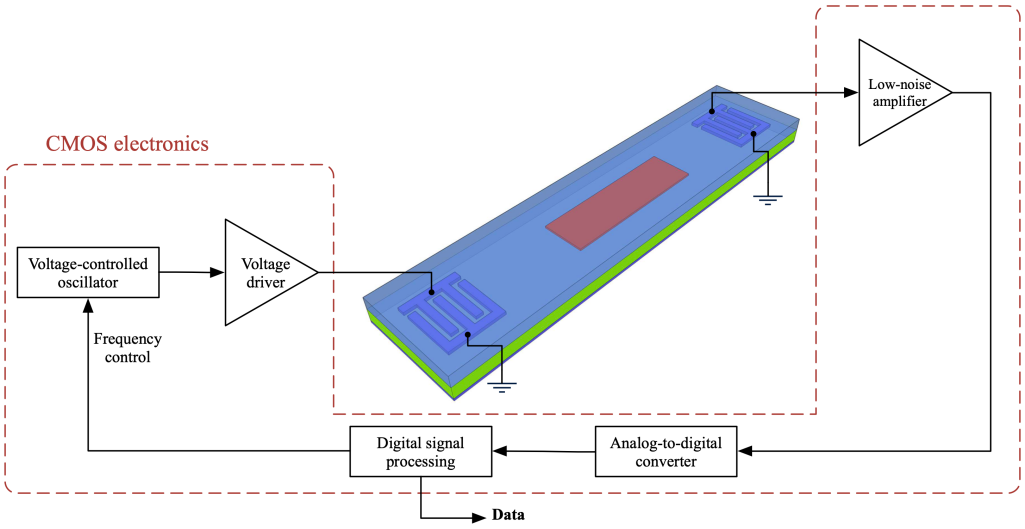


**Figure 3.7** – Block-level diagram of a possible integrated detection system.

In Figure 3.8, two alternate methods are used to apply the electrical signals to the input IDT. The first is the differential approach in which IDT are alternately connected to the negative and positive phases of a sinusoidal signal. The second is the single-ended method in which IDT are alternately connected to a single phase of a sinusoidal signal and ground. In both topologies, the bottom plane is connected to the ground.

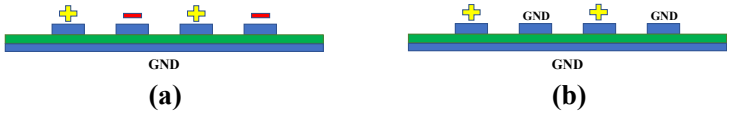


**Figure 3.8** – Illustration of the (**a**) differential and (**b**) single-ended electrode configurations, highlighting positive, negative, and ground (GND) signals.

Lin et al. have presented equivalent circuit models for different methods of applying signals for single-ended configurations, and concluded that grounding the bottom plane increases static capacitance compared to a floating plane, which improves the coupling coefficient (Lin et al., 2014).

To determine THD, a frequency simulation was first performed in COMSOL Multiphysics to find the resonance frequency of the current device configuration. Subsequently, using an input signal at the determined frequency, a 1000 ns time-dependent simulation was run with a time step of 0.01 ns. Using this time-series output voltage data, THD was calculated using MATLAB.

## 3.4 Results and Discussion

In this part, the effects of metalization ratio on different characteristics of the device are explored. In particular, its effects on gain, sensitivity, and THD in different configurations of the device are assessed. These include simulations with and without the $Si_3N_4$ layer and single-ended versus differential voltage stimulation.

The transmission gain of this device is shown in Figure 3.9. When driving the device at the resonance frequency of mode a (about 86 MHz), transmission gain is maximal at 0.0214 for a metalization ratio of 85%. When exciting mode b, with a resonance frequency of about 66 MHz, the gain reaches its maximum of 0.0144 for a ratio between 30% and 40%. Figure 3.9 suggests that mode a is optimal for a metalization ratio above 50%, whereas mode b is optimal for a metalization ratio below 50%, where the two transmission gain curves cross each other.

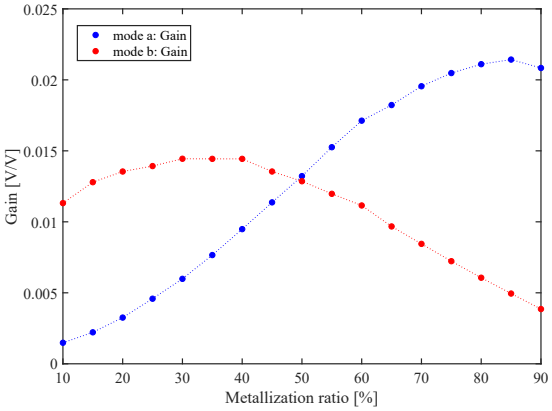


**Figure 3.9** – Transmission gain with respect to IDT metalization ratio.

Figure 3.10 presents the variations in frequency sensitivity compared to mass variation, as the IDT metalization ratio is varied from 10% to 90%. Both deformation modes explained in Section 3.2 are examined. For mode b, mass sensitivity is nearly constant for a metalization ratio ranging from 10% to 90%. In mode a,

mass sensitivity is at its maximum for an IDT metalization ratio of 10%, but is associated with a low transmission gain which would make it more challenging to discern the output signal from noise. However, for this mode, transmission gain gradually increases from a metalization ratio of 25% up to 70%, and then starts to plateau. As shown in Figure 3.10, considering the tradeoff between gain and sensitivity, the sensitivity remains mostly constant at about 114 $cm^2/g$ with 10% to 90% metalization ratios. As a point of reference, assuming a minimum detectable frequency variation of 1 Hz for the system, its sensitivity would allow a detection resolution of 1.2 ng, or the equivalent of about a hundred bacteria of typical weight (Davis et al., 1980).

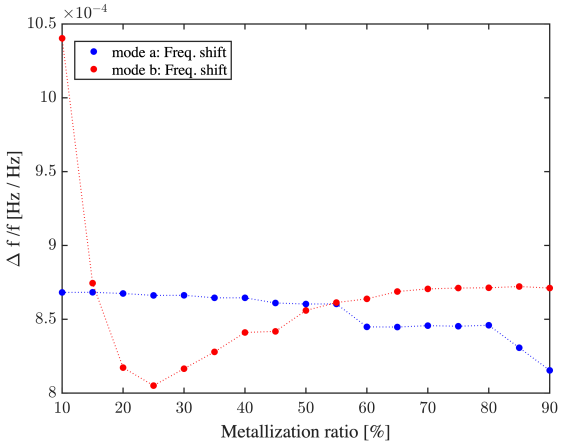


**Figure 3.10** – Sensitivity of the device depending on IDT metalization ratio in response to a 100 $kg/m^3$ increase in PMMA density.

Conventionally, metalization ratio is usually fixed at 50% which represents standard bidirectional IDT (Yantchev and Katardjiev, 2013 ; Zou et al., 2018 ; Weser et al., 2020 ; Fu et al., 2017). However, in this work, we show that it is possible to achieve a superior tradeoff between insertion loss and mass sensitivity by adjusting the metalization ratio for a given deformation mode, according to the specification priorities. For instance, in mode a, mass sensitivity is maximal for a metalization

ratio of 10%, but with poor transmission gain. However, for the same mode, a metalization ratio of 80% provides maximal transmission gain, also with reasonable mass sensitivity. As for mode b, mass sensitivity is maximal for a metalization ratio above 55%, whereas transmission gain reaches its peak at about 35%. In this case, a metalization ratio of 80% is obviously optimal.

According to the requirements of the designer, it is reasonable to establish a figure of merit (FOM) in order to optimize the selection of the metalization ratio. As a generic example, the following (plotted in Figure 3.11) attributes equal value to transmission gain and mass sensitivity :

$$\text{FOM} = \text{Transmission Gain} \times \text{Mass Sensitivity} \tag{3.3}$$

Although constituting a very simple example, the FOM could be finely adjusted according to design specifications and priorities, and could even incorporate additional performance metrics of interest (e.g., THD, power consumption, size). Figure 3.11 illustrates the ability to select an optimal metalization ratio in order to maximize a chosen FOM.

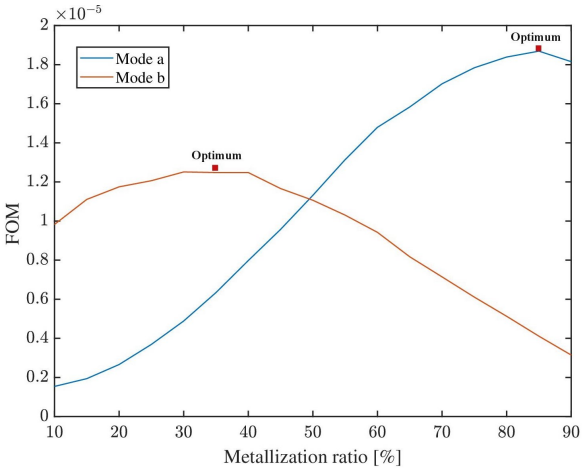


**Figure 3.11** – Arbitrary FOM shows the ability to optimize by means of metalization ratio.

All subsequent results were obtained using an input frequency of 86 MHz (mode a). In Section 3.2, two methods of applying the input signal were presented : single-ended (typical) and differential. To perform a fair comparison, the amplitude of the input signal in the single-ended configuration was doubled (10 V) compared to the differential (5 V). As shown in Figure 3.12, the differential configuration moderately improved transmission gain, reaching a maximum of 0.0235 for a metalization ratio of 85%. In the single-ended method, the maximum gain was 0.02 for a metalization ratio of 90%.

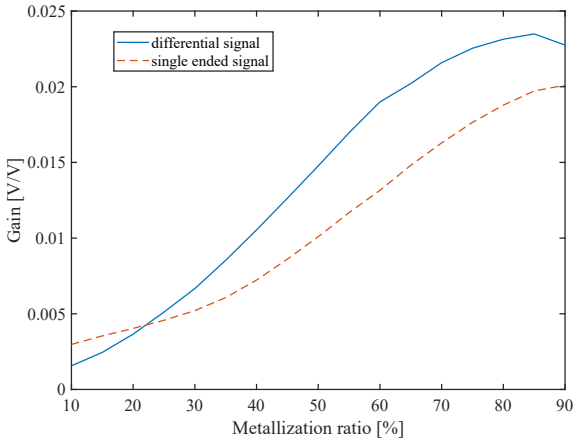


**Figure 3.12** – Device gain of single-ended and differential mode for metalization ratios ranging from 10% to 90% operating in mode a.

The physical properties of all layers play major roles in acoustic sensing : a small

thickness variation in the stack of materials could affect insertion loss (transmission gain) and sensitivity. Figure 3.13 shows that the $Si_3N_4$ layer has a significant effect on transmission gain, and hence on acoustic coupling. The acoustic velocity of $Si_3N_4$ is lower than that of the piezoelectric layer (AlN), which allows $Si_3N_4$ to behave as a guiding layer that concentrates the acoustic energy in the active device (Wang et al., 1994). Without this guiding layer, the maximum transmission gain is 0.0048, whereas, with $Si_3N_4$ present, the maximum transmission gain is improved to 0.0235, i.e., a 4.8 times increase.

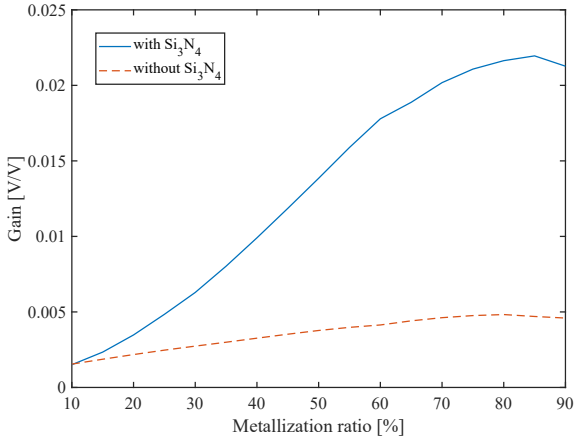


**Figure 3.13** – The effect of the $Si_3N_4$ layer on the device's gain for metalization ratios ranging from 10% to 90% operating in mode a.

When adjusting the IDT metalization ratio to optimize sensor characteristics such

as mass sensitivity and transmission gain, a serious worry is that any geometrical asymmetry might affect the shape of the generated waveform, and thus adversely impact system linearity. These concerns are alleviated in Figure 3.14, which demonstrates that THD remains stable across metalization ratios and inferior to a very low value of -108 dB, regardless of metalization ratio.

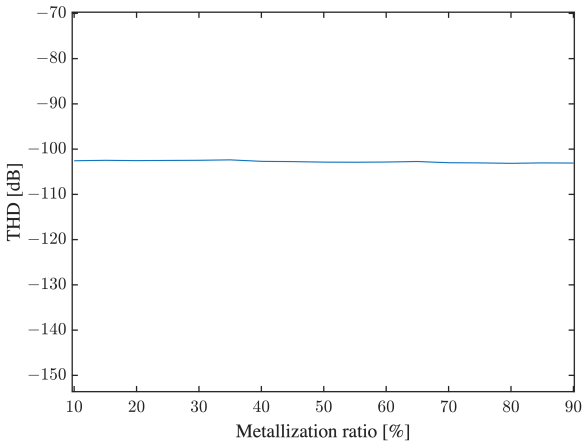


**Figure 3.14** – The effect of IDT's metalization ratio on the device's THD operating in mode a.

THD was calculated by applying Equation 3.2 to the stabilized portion of the output time series of the simulated device. For example, in Figure 3.6, outputs between 400 and 900 ns was used. Confirming the linearity of the system, Figure 3.6b shows a smooth harmonic output exempt of any visible distortion.

Table 3.2 presents the performance of the design of this work, in relation to acoustic sensors from the literature. Specifically, mass sensitivity ($S_m$) and insertion loss (IL) are compared. Insertion loss can be calculated from the transmission gain using

$$\text{Insertion loss (dB)} = 10\log_{10}\frac{|V_i|^2}{|V_o|^2} = 20\log_{10}\frac{|V_i|}{|V_o|} = 20\log_{10}\frac{1}{\text{gain}}. \qquad (3.4)$$

With FOM chosen as the ratio between mass sensitivity and insertion loss, two versions of the design of this work for different IDT metalization ratios were evaluated : one minimizing insertion loss and the other maximizing mass sensitivity. Both proposed designs were found to be reasonably competitive with the state of the art, despite the use of non-optimized commercial technology with set material properties and thicknesses.

**Table 3.2** – Comparison of acoustic wave sensors' performance.

| **Biosensor type** | $S_m$ **[cm$^2$/g]** | **IL [dB]** | $S_m$**/IL** | **Piezo Material** | **Reference** |
|---|---|---|---|---|---|
| SAW | 2.6–121.7 | 25–55 | 1.196 | ZnO | (Xu and Li, 2021) |
| SAW | - | 52.5–53.25 | - | ZnO/quartz | (Xu and Li, 2021) |
| SAW | 70 | - | - | ZnO/LiTaO3 | (Powell et al., 2004a) |
| FPW | 60.16–70.06 | 36.04 | 1.944 | ZnO | (Lan et al., 2016) |
| LW | 160–240 | - | - | AlN | (Reusch et al., 2018) |
| LW | 91.65 | 18.53 | 4.946 | ZnO | (Liu et al., 2011) |
| LW(A0) | 175.8 | 45 | 3.907 | AlN | (Li et al., 2008) |
| LW(A0 & S0) | 174–272 | 20–38 | 13.6 | GaN | (Lu et al., 2013) |
| **LW (Min IL)** | 114 | 26.74 | 4.263 | AlN | This work |
| **LW (Max $S_m$)** | 140 | 66.02 | 2.12 | AlN | This work |

## 3.5 Conclusions

This work presented the design and simulation of a mass sensitive lamb wave microsensor in the CMOS-based technology provided by SilTerra. It was shown that the $Si_3N_4$ layer present in the technology could provide a fivefold improvement in transmission gain by serving as a guiding layer. The designed devices were analyzed in two different resonant modes (around 66 and 86 MHz). It was established that the metalization ratio can be adjusted in order to achieve an

optimal tradeoff between transmission gain and sensitivity, depending on design criteria. It was also determined that the input IDT differential configuration is marginally more efficient than the single-ended one, with a 20% greater transmission gain. Worries about metalization ratio having any influence on output signal THD were unfounded, with very low levels ($-100$ dB) for all ratios. Although FEM simulation results can admittedly differ from practical results due to material parameters, mesh structure, and physics simplifications, this work was able to present a general methodology for acoustic wave sensor optimization based on structural topology. Although results may vary according to technology and device type, the general approach remains valid and worthwhile. Physical devices, currently in the fabrication pipeline, will be tested as soon as possible in order to validate this work's conclusions.

# CHAPTER IV

# CONCLUSION

In this thesis we reviewed the theory and properties of multiple acoustic biosensors with various wave propagation characteristics and compared them with each other. In order to design a mass sensitive lamb wave biosensor with existing commercial technology, SilTerra's CMOS technology properties was used in our simulations and design. In chapter 3, design and modeling of a mass sensitive lamb wave biosensor have been demonstrated. This work looked at how the IDT structure and piezoelectric thickness affected the device's characteristics, and it also showed how to model a mass-sensitive lamb wave biosensor. The designed lamb wave biosensor produced an approximate mass sensitivity of 114 $[cm^2]$/gr. Numerous time-domain and frequency-domain simulations have been run in order to get results that may be trusted. It was shown that the SilTerra technology's $Si_3N_4$ layer may be successfully used as a guiding layer to increase transmission gain by a factor of five. After examining the THD level at several IDT metallization ratios, we found that THD is incredibly low at all ratios and shouldn't be a point of concern when choosing the best metallization ratio. We found also that the metallization ratio may be effectively adjusted to give the greatest possible trade off between transmission gain and sensitivity in accordance with the design requirements. Furthermore, we discovered that switching from a single-ended to a differential input configuration for the IDT electrodes can boost transmission

gain by 20%.

## 4.1 Future work

The next step in performing this study would be to fabricate this device and compare simulated results of sensitivity, metallization ratio, THD, and signal application with the experimental ones. Through fabrication, it is possible to evaluate various immobilizers' efficiency as well as various antigen detection in diverse liquids. Combining microdevices is one of the exciting aspects of this technology. It would be of interest to use other micro-devices to mix the liquids containing the antibodies before routing them to the sensing area. This would provide the condition for more antibodies to reach the immobilizers, increasing the amount of antigens that can be detected and potentially improving the microsensor's sensitivity and accuracy (Gao et al., 2015). This could be achieved by including a micromixer in the microfluidic system, on the path towards a fully-integrated lab-on-a-chip. One specific example is the detection of insulin (Park et al., 2012). By combining micromixers with biosensors, insulin-antibodies will be mixed before being added to the sensing area, and more insulin-antibodies will be connected to the sensing area. Then, when the liquid containing insulin is added, the probability that it will be detected by an insulin antibody will increase, and a more accurate number will be announced to specialists, which is essential for the diagnosis.

# BIBLIOGRAPHY


Advances in on-line drinking water quality monitoring and early warning systems. Water Research, 45(2) :741–747, 2011. ISSN 0043-1354.

T.M. Adams and R.A. Layton. Introductory MEMS : Fabrication and Applications. Lecture Notes in Mathematics. Springer US, 2009. ISBN 9780387095110. URL https://books.google.ca/books?id=jXJCAAAAQBAJ.

V. Agache, G. Blanco-Gomez, F. Baleras, and P. Caillat. An embedded microchannel in a mems plate resonator for ultrasensitive mass sensing in liquid. Lab Chip, 11 :2598–2603, 2011.

KA Ahmad, Z Hussain, Z Janin, and A Abd Manaf. Piezoelectric micromachined ultrasonic transducers array based on is mode polarization method. In 2017 IEEE 4th International Conference on Smart Instrumentation, Measurement and Application (ICSIMA), pages 1–4. IEEE, 2017.

Yoshikatsu Akiyama. Design of temperature-responsive cell culture surfaces for cell sheet engineering. Cyborg and Bionic Systems, 2021, 2021.

Antonio Arnau et al. Piezoelectric transducers and applications, volume 2004. Springer, 2004.

Muhammad Zubair Aslam, Varun Jeoti, Shahid Manzoor, Mehwish Hanif, and Muhammad Junaid. An aluminium nitride based multilayer structure for love mode surface acoustic wave devices. Semiconductor Science and Technology, 35(11) :115007, sep 2020.

Ikuo Awai and Yangjun Zhang. Overlap integral calculation of resonator coupling. In 2006 12th International Symposium on Antenna Technology and Applied Electromagnetics and Canadian Radio Sciences Conference, pages 1–4, 2006.

C Caliendo and M Hamidullah. Pressure sensing with zero group velocity lamb modes in self-supported a-sic/c-zno membranes. Journal of Physics D : Applied Physics, 51(38) :385102, 2018.

C Caliendo and M Hamidullah. Guided acoustic wave sensors for liquid environments. Journal of Physics D : Applied Physics, 52(15) :153001, feb 2019.

Cinzia Caliendo, Ennio Giovine, and Muhammad Hamidullah. Design and fabrication of zero-group-velocity lamb wave resonator onto silicon nitride/aluminum nitride suspended membrane. AIP Conference Proceedings, 1990(1) :020013, 2018.

Hung-Wei Chang and Jeng-Shong Shih. Surface acoustic wave immunosensors based on immobilized c60-proteins. Sensors and Actuators B : Chemical, 121 (2) :522–529, 2007. ISSN 0925-4005.

Xi Chen, Meng Wang, and Gang Zhao. Point-of-care assessment of hemostasis with a love-mode surface acoustic wave sensor. ACS Sensors, 5(1) :282–291, 2020. doi : 10.1021/acssensors.9b02382. PMID : 31903758.

A. Choujaa, N. Tirole, C. Bonjour, G. Martin, D. Hauden, P. Blind, A. Cachard, and C. Pommier. Aln/silicon lamb-wave microsensors for pressure and gravimetric measurements. Sensors and Actuators A : Physical, 46(1) :179–182, 1995. ISSN 0924-4247.

M. Cole, G. Sehra, J.W. Gardner, and V.K. Varadan. Development of smart tongue devices for measurement of liquid properties. IEEE Sensors Journal, 4 (5) :543–550, 2004a. doi : 10.1109/JSEN.2004.832855.

M. Cole, G. Sehra, J.W. Gardner, and V.K. Varadan. Development of smart tongue devices for measurement of liquid properties. IEEE Sensors Journal, 4 (5) :543–550, 2004b. doi : 10.1109/JSEN.2004.832855.

BD Davis, R Dulbecco, HN Eiser, and HS Ginsberg. Microbiology : Including immunology and molecular genetics, harper and row. Hagerstown, Md, 19802, 1980.

Eugène Dieulesaint and Daniel Royer. Elastic waves in solids : applications to signal processing. John Wiley & Sons, 1980.

R. Duhamel, L. Robert, Hongguang Jia, Feng Li, F. Lardet-Vieudrin, J.-F. Manceau, and F. Bastien. Sensitivity of a lamb wave sensor with 2 m aln membrane. Ultrasonics, 44 :e893–e897, 2006. ISSN 0041-624X. Proceedings of Ultrasonics International (UI'05) and World Congress on Ultrasonics (WCU).

Y.Q. Fu, J.K. Luo, X.Y. Du, A.J. Flewitt, Y. Li, G.H. Markx, A.J. Walton, and W.I. Milne. Recent developments on zno films for acoustic wave based biosensing and microfluidic applications : a review. Sensors and Actuators B : Chemical, 143(2) :606–619, 2010. ISSN 0925-4005.

Y.Q. Fu, J.K. Luo, N.T. Nguyen, A.J. Walton, A.J. Flewitt, X.T Zu, Y. Li, G. McHale, A. Matthews, E. Iborra, H. Du, and W.I. Milne. Advances in

piezoelectric thin films for acoustic biosensors, acoustofluidics and lab-on-chip applications. Progress in Materials Science, 89 :31–91, 2017. ISSN 0079-6425.

Yuan Gao, Phong Tran, Karolina Petkovic-Duran, Tony Swallow, and Yonggang Zhu. Acoustic micromixing increases antibody-antigen binding in immunoassays. Biomedical microdevices, 17(4) :1–5, 2015.

Eleanor R Gray, Valérian Turbé, Victoria E Lawson, Robin H Page, Zara C Cook, R Bridget Ferns, Eleni Nastouli, Deenan Pillay, Hiromi Yatsuda, Dale Athey, et al. Ultra-rapid, sensitive and specific digital diagnosis of hiv with a dual-channel saw biosensor in a pilot clinical study. NPJ digital medicine, 1(1) :1–8, 2018.

Jose M Guisan et al. Immobilization of enzymes and cells, volume 22. Springer, 2006.

Kui Han and Yong J. Yuan. Mass sensitivity evaluation and device design of a love wave device for bond rupture biosensors using the finite element method. IEEE Sensors Journal, 14(8) :2601–2608, 2014.

Hoang-Si Hong and Gwiy-Sang Chung. Surface acoustic wave humidity sensor based on polycrystalline aln thin film coated with sol–gel derived nanocrystalline zinc oxide film. Sensors and Actuators B : Chemical, 148(2) :347–352, 2010. ISSN 0925-4005.

David A. Horsley, Ofer Rozen, Yipeng Lu, Stefon Shelton, Andre Guedes, Richard Przybyla, Hao-Yen Tang, and Bernhard E. Boser. Piezoelectric micromachined ultrasonic transducers for human-machine interfaces and biometric sensing. In 2015 IEEE SENSORS, pages 1–4, 2015. doi : 10.1109/ICSENS.2015.7370564.

M. Zakir Hossain and Natsuhiko Shimizu. Covalent immobilization of gold nanoparticles on graphene. The Journal of Physical Chemistry C, 123(6) :3512–3516, 2019.

Youju Huang, Palanisamy Kannan, Lei Zhang, Tao Chen, and Dong-Hwan Kim. Concave gold nanoparticle-based highly sensitive electrochemical igg immunobiosensor for the detection of antibody–antigen interactions. RSC Adv., 5 : 58478–58484, 2015.

B. T. Khuri-Yakub, K. K. Park, H. J. Lee, G. G. Yaralioglu, S. Ergun, O. Oralkan, M. Kupnik, C. F. Quate, T. Braun, H. P. Lang, M. Hegner, J.-P. Ramseyer, C. Gerber, and J. Gimzewski. 6d-1 the capacitive micromachined ultrasonic transducer (cmut) as a chem/bio sensor. In 2007 IEEE Ultrasonics Symposium Proceedings, pages 472–475, 2007. doi : 10.1109/ULTSYM.2007.127.

Butrus T Khuri-Yakub and Ömer Oralkan. Capacitive micromachined ultrasonic transducers for medical imaging and therapy. Journal of micromechanics and microengineering, 21(5) :054004, 2011.

Rahul Kishor, Fei Gao, Sivaramapanicker Sreejith, Xiaohua Feng, Yen Peng Seah, Zhenfeng Wang, Mihaiela Corina Stuparu, Teik-Thye Lim, Xiaodong Chen, and Yuanjin Zheng. Photoacoustic induced surface acoustic wave sensor for concurrent opto-mechanical microfluidic sensing of dyes and plasmonic nanoparticles. RSC Adv., 6 :50238–50244, 2016.

Hui Kong, Chuanyu Li, Zhen Guo, Wei Zhang, Jia Yao, Hongnan Zhu, Ruhong Yan, Lirong Wang, Jinze Li, Wei Wei, and Lianqun Zhou. Sensitivity improved with parylene-c passivized on lamb wave sensor for aptt measurement through monitoring whole blood reaction. Sensors and Actuators B : Chemical, 285 : 479–486, 2019. ISSN 0925-4005.

Ashok Kumar et al. Biosensors based on piezoelectric crystal detectors : theory and application. JOM-e, 52(10) :1–6, 2000.

IE Kuznetsova, AV Smirnov, Yu V Plekhanova, AN Reshetilov, and G-J Wang. Effect of the aperture of an interdigital transducer on the characteristics of its output signal in a piezoelectric plate. Bulletin of the Russian Academy of Sciences : Physics, 84(6) :644–647, 2020.

Iren E Kuznetsova, Vladimir I Anisimkin, Sergei P Gubin, Sergei V Tkachev, Vladimir V Kolesov, Vadim V Kashin, Boris D Zaitsev, Alexander M Shikhabudinov, Enrico Verona, and Shaorong Sun. Super high sensitive plate acoustic wave humidity sensor based on graphene oxide film. Ultrasonics, 81 :135–139, 2017.

Ming-Liang Lai. Developing Piezoelectric Biosensing Methods. PhD thesis, Glasgow Theses Service, 2015.

Je-Wei Lan, I-Yu Huang, Yu-Cheng Lin, Chang-Yu Lin, Jian-Lin Chen, and Chia-Hsu Hsieh. Development of an fpw biosensor with low insertion loss and high fabrication yield for detection of carcinoembryonic antigen. Sensors, 16(11), 2016. ISSN 1424-8220.

Chi-Yuan Lee, Chia-Chieh Shen, Shuo-Jen Lee, Chun-Wei Chiu, and Hsiang-Ting Lin. Real-time microscopic monitoring of temperature and strain on the surface of magnesium hydrogen storage tank by high temperature resistant flexible integrated microsensor. International Journal of Hydrogen Energy, 47(25) : 12815–12821, 2022. ISSN 0360-3199.

Feng Li, Yi-hui Wu, J. F. Manceau, and F. Bastien. Multi-parameter sensing in liquid using a lamb wave based microsensor. In 2008 Symposium on Piezoelectricity, Acoustic Waves, and Device Applications, pages 320–323, 2008.

Chih-Ming Lin, Ventsislav Yantchev, Jie Zou, Yung-Yu Chen, and Albert P. Pisano. Micromachined one-port aluminum nitride lamb wave resonators utilizing the lowest-order symmetric mode. Journal of Microelectromechanical Systems, 23(1) :78–91, 2014.

Mengwei Liu, Junhong Li, Jun Ma, and Chenghao Wang. Design and fabrication of a MEMS lamb wave device based on ZnO thin film. Journal of Semiconductors, 32(4) :044006, apr 2011.

Xing Lu, Chi Ming Lee, Shu Yuen Wu, Ho Pui Ho, and Kei May Lau. Gan-based $s_0$ -wave sensors on silicon for chemical and biological sensing in liquid environments. IEEE Sensors Journal, 13(4) :1245–1251, 2013. doi : 10.1109/JSEN.2012.2231958.

Ralf Lucklum, David Soares, and Kay Kanazawa. Models for Resonant Sensors, pages 69–99. Springer Berlin Heidelberg, Berlin, Heidelberg, 2004. ISBN 978-3-662-05361-4. doi : 10.1007/978-3-662-05361-4_4. URL https://doi.org/10.1007/978-3-662-05361-4_4.

Jingting Luo, Pingxiang Luo, Min Xie, Ke Du, Bixia Zhao, Feng Pan, Ping Fan, Fei Zeng, Dong ping Zhang, Zhuang-hao Zheng, and Guangxing Liang. A new type of glucose biosensor based on surface acoustic wave resonator using mn-doped zno multilayer structure. Biosensors & bioelectronics, 49 :512–8, 2013.

Aamir F. Malik, Varun Jeoti, Mohamad Fawzy, Asif Iqbal, Zubair Aslam, Mohanraj Soundara Pandian, and Eloi Marigo. Estimation of saw velocity and coupling coefficient in multilayered piezo-substrates aln/sio<inf>2</inf>/si. In 2016 6th International Conference on Intelligent and Advanced Systems (ICIAS), pages 1–5, 2016.

S.J. Martin, A.J. Ricco, T.M. Niemczyk, and G.C. Frye. Characterization of sh acoustic plate mode liquid sensors. Sensors and Actuators, 20(3) :253–268, 1989. ISSN 0250-6874. doi : https://doi.org/10.1016/0250-6874(89)80124-6. URL https://www.sciencedirect.com/science/article/pii/0250687489801246.

T. Moriizumi, Y. Unno, and S. Shiokawa. New sensor in liquid using leaky saw. In IEEE 1987 Ultrasonics Symposium, pages 579–582, 1987. doi : 10.1109/ULTSYM.1987.199023.

Adnan Mujahid and Franz L. Dickert. Surface acoustic wave (saw) for chemical sensing applications of recognition layers. Sensors, 17(12), 2017. ISSN 1424-8220. doi : 10.3390/s17122716. URL https://www.mdpi.com/1424-8220/17/12/2716.

Minu Prabhachandran Nair, Adrian JT Teo, and King Ho Holden Li. Acoustic biosensors and microfluidic devices in the decennium : Principles and applications. Micromachines, 13(1) :24, 2021.

H. Nakamura, H. Nakanishi, T. Tsurunari, K. Matsunami, and Y. Iwasaki. 6e-1 a small-sized saw duplexer on a sio2/idt/linbo3 structure for wideband cdma application. In 2007 IEEE Ultrasonics Symposium Proceedings, pages 488–491, 2007.

Jeonghun Nam, Woong Sik Jang, Jisu Kim, Hyukjin Lee, and Chae Seung Lim. Lamb wave-based molecular diagnosis using dna hydrogel formation by rolling circle amplification (rca) process. Biosensors and Bioelectronics, 142 :111496, 2019. ISSN 0956-5663.

Haleh Nazemi, Aashish Joseph, Jaewoo Park, and Arezoo Emadi. Advanced micro- and nano-gas sensor technology : A review. Sensors, 19(6) :1285, 2019.

Haruka Oda, Kazunori Kihara, Y Morimoto, and S Takeuchi. Cell-based biohybrid sensor device for chemical source direction estimation. Cyborg and Bionic Systems, 2021, 2021.

A. K. Pantazis, E. Gizeli, and G. Konstantinidis. A high frequency gan lamb-wave sensor device. Applied Physics Letters, 96(19) :194103, 2010.

Alexandros K. Pantazis, Georgios Konstantinidis, and Electra Gizeli. Characterization of a gan lamb-wave sensor for liquid-based mass sensing applications. IEEE Sensors Journal, 14(3) :908–911, 2014. doi : 10.1109/JSEN.2013.2291393.

Mohammad Salemizadeh Parizi, Fatemeh Salemizadehparizi, Mahdi Molaei Zarasvand, Saeed Abdolhosseini, Shahram Bahadori-Haghighi, and Alireza Khalilian. High-performance graphene-based biosensor using a metasurface of asymmetric silicon disks. IEEE Sensors Journal, 22(3) :2037–2044, 2022. doi : 10.1109/JSEN.2021.3134205.

Jungwook Park, Stanislav L. Karsten, Shuhei Nishida, Hideki Kawakatsu, and Hiroyuki Fujita. Application of a new microcantilever biosensor resonating at the air–liquid interface for direct insulin detection and continuous monitoring of enzymatic reactions. Lab Chip, 12 :4115–4119, 2012. doi : 10.1039/C2LC40232G. URL http://dx.doi.org/10.1039/C2LC40232G.

Michele Penza, Patrizia Aversa, Gennaro Cassano, Domenico Suriano, Wojtek Wlodarski, Massimiliano Benetti, Domenico Cannata, Fabio Di Pietrantonio, and Enrico Verona. Thin-film bulk-acoustic-resonator gas sensor functionalized with a nanocomposite langmuir–blodgett layer of carbon nanotubes. IEEE Transactions on Electron Devices, 55(5) :1237–1243, 2008. doi : 10.1109/TED.2008.919283.

Luigi Piro, Leonardo Lamanna, Francesco Guido, Antonio Balena, Massimo Mariello, Francesco Rizzi, and Massimo De Vittorio. Flexible saw microfluidic devices as wearable ph sensors based on zno nanoparticles. Nanomaterials, 11 (6), 2021. ISSN 2079-4991.

Miroslav Pohanka. The piezoelectric biosensors : Principles and applications. Int. J. Electrochem. Sci, 12 :496–506, 2017.

Miroslav Pohanka. Overview of piezoelectric biosensors, immunosensors and dna sensors and their applications. Materials, 11(3), 2018. ISSN 1996-1944.

David A. Powell, Kourosh Kalantar-zadeh, and Wojtek Wlodarski. Numerical calculation of saw sensitivity : application to zno/litao3 transducers. Sensors and Actuators A : Physical, 115(2) :456–461, 2004a. ISSN 0924-4247. The 17th European Conference on Solid-State Transducers.

David A. Powell, Kourosh Kalantar-zadeh, and Wojtek Wlodarski. Numerical calculation of saw sensitivity : application to zno/litao3 transducers. Sensors and Actuators A : Physical, 115(2) :456–461, 2004b. ISSN 0924-4247. doi : https://doi.org/10.1016/j.sna.2004.05.031. URL https://www.sciencedirect.com/science/article/pii/S0924424704003929. The 17th European Conference on Solid-State Transducers.

Abhinav Prasad, Ashwin A. Seshia, and Jérôme Charmet. Micromechanical piezoelectric-on-silicon baw resonators for sensing in liquid environments. In 2015 Joint Conference of the IEEE International Frequency Control Symposium the European Frequency and Time Forum, pages 209–213, 2015. doi : 10.1109/FCS.2015.7138825.

Jin Qian, Cuiping Li, Lirong Qian, Mingji Li, Hongji Li, and Baohe Yang. Three-dimensional finite element simulation of love mode surface acoustic wave in layered structures including zno piezoelectric film and diamond substrate. Diamond and Related Materials, 88 :123–128, 2018. ISSN 0925-9635.

Yongqiang Qiu, James V. Gigliotti, Margeaux Wallace, Flavio Griggio, Christine E. M. Demore, Sandy Cochran, and Susan Trolier-McKinstry. Piezoelectric

micromachined ultrasound transducer (pmut) arrays for integrated sensing, actuation and imaging. Sensors, 15(4) :8020–8041, 2015. ISSN 1424-8220. doi : 10.3390/s150408020. URL https://www.mdpi.com/1424-8220/15/4/8020.

Markus Reusch, Katarzyna Holc, Vadim Lebedev, Nicolas Kurz, Agnė Žukauskaitė, and Oliver Ambacher. Temperature cross-sensitivity of aln-based flexural plate wave sensors. IEEE Sensors Journal, 18(19) :7810–7818, 2018.

María Isabel Gaso Rocha, Yolanda Jiménez, Francis A. Laurent, and Antonio Arnau. Love wave biosensors : A review. In Toonika Rinken, editor, State of the Art in Biosensors, chapter 11. IntechOpen, Rijeka, 2013.

María-Isabel Rocha-Gaso, Carmen March-Iborra, Ángel Montoya-Baides, and Antonio Arnau-Vives. Surface generated acoustic wave biosensors for the detection of pathogens : A review. Sensors, 9(7) :5740–5769, 2009a. ISSN 1424-8220. doi : 10.3390/s90705740. URL https://www.mdpi.com/1424-8220/9/7/5740.

María-Isabel Rocha-Gaso, Carmen March-Iborra, Ángel Montoya-Baides, and Antonio Arnau-Vives. Surface generated acoustic wave biosensors for the detection of pathogens : A review. Sensors, 9(7) :5740–5769, 2009b. ISSN 1424-8220. doi : 10.3390/s90705740. URL https://www.mdpi.com/1424-8220/9/7/5740.

Katsuhisa Sakaguchi, Kei Akimoto, Masanori Takaira, Ryu-ichiro Tanaka, Tatsuya Shimizu, and Shinjiro Umezu. Cell-based microfluidic device utilizing cell sheet technology. Cyborg and Bionic Systems, 2022, 2022.

Zaid T. Salim, U. Hashim, M.K.Md. Arshad, Makram A. Fakhri, and Evan T. Salim. Frequency-based detection of female aedes mosquito using surface acoustic wave technology : Early prevention of dengue fever. Microelectronic Engineering, 179 :83–90, 2017. ISSN 0167-9317. doi : https://doi.org/10.1016/j.mee.2017.04.016. URL https://www.sciencedirect.com/science/article/pii/S0167931717301454.

Abdollah Vaez Shoushtari. Seismic Hazard Assessment of Peninsular Malaysia Based on New Ground Motion Prediction Equations for Subduction Earthquakes. PhD thesis, Universiti Teknologi Malaysia, 2016.

J.L. Skinner, G.F. Cardinale, A.A. Talin, and R.W. Brocato. Effect of critical dimension variation on saw correlator energy. IEEE Transactions on Ultrasonics, Ferroelectrics, and Frequency Control, 53(2) :497–501, 2006.

Taehyeon Song, Seung Yeon Song, Hyun C. Yoon, and Keekeun Lee. Development of a wireless love wave biosensor platform for multi-functional detection. Japanese Journal of Applied Physics, 50(6) :06GL09, jun 2011. doi : 10.1143/jjap.50.06gl09. URL https://doi.org/10.1143/jjap.50.06gl09.

Ananth Sridhar. Anatomy of a piezoelectric micromachined ultrasonic transducer, Feb 2020. URL https://onscale.com/blog/anatomy-of-a-piezoelectric-micromachined-ultrasonic-transducer/.

A.K. Srivastava, N. Dwivedi, C. Dhand, R. Khan, N. Sathish, M.K. Gupta, R. Kumar, and S. Kumar. Potential of graphene-based materials to combat covid-19 : properties, perspectives, and prospects. Materials Today Chemistry, 18 :100385, 2020. ISSN 2468-5194. doi : https://doi.org/10.1016/j.mtchem.2020.100385. URL https://www.sciencedirect.com/science/article/pii/S2468519420301452.

Ollivier Tamarin, Maxence Rube, Jean Luc Lachaud, Vincent Raimbault, Dominique Rebière, and Corinne Dejous. Mobile acoustic wave platform deployment in the amazon river : Impact of the water sample on the love wave sensor response. Sensors, 20(1), 2020. ISSN 1424-8220.

DP Tang, R Yuan, YQ Chai, X Zhong, Y Liu, JY Dai, and LY Zhang. Novel potentiometric immunosensor for hepatitis b surface antigen using a gold nanoparticle-based biomolecular immobilization method. Analytical biochemistry, 333(2) :345—350, October 2004. ISSN 0003-2697. doi : 10.1016/j.ab.2004.06.035.

Onur Tigli, Louis Bivona, Patricia Berg, and Mona Zaghloul. Fabrication and characterization of a surface-acoustic-wave biosensor in cmos technology for cancer biomarker detection. Biomedical Circuits and Systems, IEEE Transactions on, 4 :62 – 73, 03 2010. doi : 10.1109/TBCAS.2009.2033662.

Shyam Trivedi and Harshal B. Nemade. Finite element simulation of love wave resonator for dna detection. International Journal of Advances in Engineering Sciences and Applied Mathematics, 7(4) :210–218, 2015. ISSN 0975-5616.

IA Viktrov. Rayleigh and lamb waves : physical theory and applications. Chapter II, 1967.

Marina V Voinova. On mass loading and dissipation measured with acoustic wave sensors : A review. Journal of Sensors, 2009, 2009.

Z. Wang, J. David N. Cheeke, and Cheng Kuei Jen. Sensitivity analysis for love mode acoustic gravimetric sensors. Applied Physics Letters, 64 :2940–2942, 1994.

N. Weckman and A. Seshia. Flexural plate wave devices and fluidic system for protein sensing in liquid. In 2017 IEEE SENSORS, pages 1–3, 2017. doi : 10.1109/ICSENS.2017.8234388.

S.W. Wenzel and R.M. White. A multisensor employing an ultrasonic lamb-wave oscillator. IEEE Transactions on Electron Devices, 35(6) :735–743, 1988.

R. Weser, A. Winkler, M. Weihnacht, S. Menzel, and H. Schmidt. The complexity of surface acoustic wave fields used for microfluidic applications. Ultrasonics, 106 :106160, 2020. ISSN 0041-624X.

C. Willberg, S. Duczek, J. M. Vivar-Perez, and Z. A. B. Ahmad. Simulation Methods for Guided Wave-Based Structural Health Monitoring : A Review. Applied Mechanics Reviews, 67(1), 01 2015. ISSN 0003-6900. doi : 10.1115/1.4029539. URL https://doi.org/10.1115/1.4029539. 010803.

G Wingqvist, L Arapan, V Yantchev, and I Katardjiev. A micromachined thermally compensated thin film lamb wave resonator for frequency control and sensing applications. Journal of Micromechanics and Microengineering, 19(3) : 035018, feb 2009.

Hank Wohltjen. Mechanism of operation and design considerations for surface acoustic wave device vapour sensors. Sensors and Actuators, 5(4) :307–325, 1984. ISSN 0250-6874.

Junru Wu and Zhemin Zhu. Sensitivity of lamb wave sensors in liquid sensing. IEEE Transactions on Ultrasonics, Ferroelectrics, and Frequency Control, 43 (1) :71–72, 1996.

Wencheng Xu, Xu Zhang, Seokheun Choi, and Junseok Chae. A high-quality-factor film bulk acoustic resonator in liquid for biosensing applications. Journal of Microelectromechanical Systems, 20(1) :213–220, 2011. doi : 10.1109/JMEMS.2010.2093568.

Zhangliang Xu and Zhifeng Li. Design and fabrication of zno-based saw sensor using low power homo-buffer layer for enhanced humidity sensing. IEEE Sensors Journal, 21(6) :7428–7433, 2021.

V. Yantchev, L. Arapan, I. Ivanov, I. Uzunov, I. Katardjiev, and V. Plessky. Parametric study of thin-film zero-group velocity resonators (zgvr). In 2012 IEEE International Ultrasonics Symposium, pages 307–310, 2012. doi : 10.1109/ULTSYM.2012.0075.

Ventsislav Yantchev and Ilia Katardjiev. Thin film lamb wave resonators in frequency control and sensing applications : a review. Journal of Micromechanics and Microengineering, 23(4) :043001, mar 2013.

Ventsislav Yantchev, Lilia Arapan, Ilia Katardjiev, and Victor Plessky. Thin-film zero-group-velocity lamb wave resonator. Applied Physics Letters, 99(3) : 033505, 2011.

Jyh-Cheng Yu and Jong-Xin Tsai. Design and manufacturing of lamb-wave biosensors using pzt on sin thin film.

Lawrence Yule, Bahareh Zaghari, Nicholas Harris, and Martyn Hill. Modelling and validation of a guided acoustic wave temperature monitoring system. Sensors, 21(21) :7390, 2021.

Iván Zamora, Eyglis Ledesma, Arantxa Uranga, and Núria Barniol. Monolithic single pmut-on-cmos ultrasound system with +17 db snr for imaging applications. IEEE Access, 8 :142785–142794, 2020.

Guangdong Zhan, Wentong Wang, Hongyan Sun, Yaxin Hou, and Lin Feng. Autocsc : A transfer learning based automatic cell segmentation and count framework. Cyborg and Bionic Systems, 2022, 2022.

Feng Zhang, Shuangming Li, Kang Cao, Pengjuan Wang, Yan Su, Xinhua Zhu, and Ying Wan. A microfluidic love-wave biosensing device for psa detection based on an aptamer beacon probe. Sensors, 15(6) :13839–13850, 2015. ISSN 1424-8220.

Junyu Zhang, Xiaojing Zhang, Xinwei Wei, Yingying Xue, Hao Wan, and Ping Wang. Recent advances in acoustic wave biosensors for the detection of disease-related biomarkers : A review. Analytica Chimica Acta, 1164 :338321, 2021a.

Junyu Zhang, Xiaojing Zhang, Xinwei Wei, Yingying Xue, Hao Wan, and Ping Wang. Recent advances in acoustic wave biosensors for the detection of disease-related biomarkers : A review. Analytica Chimica Acta, 1164 :338321, 2021b. ISSN 0003-2670.

Jie Zou, Chih-Ming Lin, C. S. Lam, and Albert P. Pisano. Transducer design for aln lamb wave resonators. Journal of Applied Physics, 121(15) :154502, 2017.

Jie Zou, Chih-Ming Lin, Anming Gao, and Albert P. Pisano. The multi-mode resonance in aln lamb wave resonators. Journal of Microelectromechanical Systems, 27(6) :973–984, 2018.